WAVES IN RANDOM AND COMPLEX MEDIA

https://www.tandfonline.com/journals/twrm20

Impact factor = 4.853

ACCEPTED OCTOBER 17TH 2022

INFLUENCE OF VARIABLE THERMAL CONDUCTIVITY AND DISSIPATION ON MAGNETIC CARREAU FLUID FLOW ALONG A MICRO-CANTILEVER SENSOR IN A SQUEEZING REGIME

R K V Muhammed [1], Hussain Basha[1], G J Reddy[1,*], Usha Shankar[2] and O. Anwar Bég[3]

[1]Laboratory on Computational Fluid Dynamics, Department of Mathematics, Central University of Karnataka, Kalaburagi-585 367, Karnataka, India.

[2]Karnataka Power Corporation Limited, Raichur Thermal Power Station, Shaktinagar-584 170, India.

[3]Professor, Multi-physical Engineering Sciences, Aeronautical/Mechanical Engineering Department, School of Science, Engineering and Environment, Salford University, Manchester M54WT, UK.

* *Corresponding author email: gjr@cuk.ac.in*

ABSTRACT

Mathematical modelling of squeezing flows finds numerous applications in biological, mechanical and medical engineering. Sensors feature such flows and can be effectively utilized to control vibrations and regulate lubrication. Magnetic fluids are critical to modern sensor systems. Micro-cantilevers are utilized in biomedical applications as biological, physical or chemical sensors and operate via detection of variations in the vibrational frequency or cantilever bending. In the present article, motivated by the deployment of intelligent electromagnetic rheological liquids in biomedical sensor systems, a theoretical study is conducted to explore the dissipative flow and thermal characteristics in non-Newtonian boundary layer flow along a micro-cantilever sensor surface suspended in a squeezing regime between parallel plates. To accurately simulate the non-Newtonian characteristics of magneto-rheological lubricants, the Carreau viscoelastic fluid model is deployed. Heat transfer is also considered to quantify thermal behaviour of sensor surfaces under squeezing conditions in the presence of Lorentz magnetohydrodynamic (MHD) body forces. Furthermore, to achieve a more refined simulation, the effects of variable thermal conductivity and Joule magnetic dissipation are incorporated. The governing conservation equations for unsteady magnetic Carreau squeezing flow and heat transfer are rendered dimensionless and self-similar via appropriate scaling transformations. The emerging nonlinear coupled boundary value problem is then solved with an efficient numerical method (Runge-Kutta 4th order shooting technique in MATLAB software). Validation of solutions with earlier simpler models over a range of Prandtl numbers and squeezing parameter values is included. Comprehensive analysis and extensive graphical visualization is included in order to quantify the thermal and hydrodynamic behaviour for the influence of key emerging parameters. It is identified that magnifying Weissenberg (viscoelastic) parameter decays the flow field. Enhancing squeezing flow parameter (plate gap parameter) decelerates the flow and decreases temperatures. Temperatures are boosted with increment in the thermal conductivity parameter and Eckert number. Skin friction is elevated with increasing Carreau power-law index and Weissenberg number. Local Nusselt number is also enhanced with larger values of thermal conductivity parameter and Eckert number (i. e. stronger viscous and Joule heating effects). The novelty of the present study is the inclusion of dissipation and thermal conductivity variation effects which extends previous investigations and provides a more accurate appraisal of thermal characteristics in sensor squeezing flows.

KEYWORDS: *Smart sensors; Carreau fluid; Micro-Cantilever, Weissenberg parameter; Magnetic field; Squeezing flow; Boundary layer; Free stream; Variable thermal conductivity; Dissipation; MATLAB.*

NOMENCLATURE:

$\boldsymbol{b}$ Plate gap parameter (squeezing flow index parameter)
$\boldsymbol{M}$ Magnetic body force number
$\boldsymbol{n}$ Carreau power-law rheological index
$\boldsymbol{We}$ Weissenberg number
$\boldsymbol{f_o}$ Permeable wall transpiration (suction/injection velocity) parameter
$\boldsymbol{Ec}$ Eckert number
$\boldsymbol{Pr}$ Prandtl number
$H(t)$ plate separation distance
k Thermal conductivity
t Dimensional time
T Dimensional temperature
u, v Dimensional velocity components
f, f' Dimensionless velocity components
x, y Axial and normal coordinates

Greek letters

α Thermal diffusivity
μ Dynamic viscosity
ρ Density
ν Kinematic viscosity
θ Dimensionless temperature
ψ Dimensionless stream function

Subscripts

w Wall conditions
∞ Ambient conditions

1. INTRODUCTION

In the rapid development of modern fluid dynamics technologies, mathematical models of thermo-fluid transport are contributing an increasingly significant role in optimizing the performance of industrial and engineering systems including biophysical devices, nuclear reactor cooling, coating systems, energy production and biotechnology. Heat transfer in viscous flows features frequently in biomedicine in for example blood flow in arteries and capillaries, magnetic drug targeting, skin comfort, burn injury, laser treatment of eye diseases etc. In many medical and industrial applications, heat transfer also arises in lubrication e. g. synovial performance, biomaterials manufacturing, injection molding for medical prosthetics etc. A common type of flow regime encountered is *nonlinear squeezing flow* [1] in which surfaces approach each other and are separated by a thin intercalating lubricant layer to absorb loads and dissipate vibrations. Many excellent studies have been communicated on squeezing flows both for Newtonian and non-Newtonian fluids [2, 3]. Such flows are also attractive as they provide an opportunity for solving reduced versions of the Navier-Stokes equations via suitable transformations.

In modern chemical and biomedical technology, a *microcantilever with sensor surfaces* is often deployed in the detection of different human diseases, harmful materials and bio-warfare agents. The micro-cantilever bends much like a “diving board”. It has a coated receiver on its surfaces and is a parallel-plate structural system with an intercalated thin film layer subjected to squeezing. The sensor operates via the bending stresses or vibrational frequency. The squeezed film layer is often rheological in nature and different models are available to account for the non-Newtonian characteristics. Various uses of microcantilevers in biomedicine are documented in Zhang *et al*. [4].

Many excellent studies of Newtonian viscous squeezing flow between approaching plates have been reported, including Gupta *et al.* [5]. Kuzma [7] experimentally demonstrated the influence of inertial force on squeezing flow between parallel plates. Squeezing viscous flow between elliptic plates was addressed analytically by Wang and Watson [8]. The study in [8] was generalized by Usha and Sridharan [9] who considered time-dependent approach distance between the plates engulfing a viscous Newtonian squeeze film. Petrov and Kharlamova [9] presented asymptotic solutions (in terms of Reynolds number) for viscous Newtonian fluid between two parallel plates, one stationary and the other moving away or towards the stationary plate. They considered the gap between plate's changes to vary with a power-law time function and also identified a critical Reynolds number associated with counterflow in the squeeze regime. Mustafa *et al.* [10] used a homotopy analysis method to extend the above studies by including thermal and species diffusion in time-dependent squeezing transport.

The above studies used the classical Newtonian model which cannot adequately describe the complex non-Newtonian properties of micro-cantilever lubricants. Many rheological squeezing flows studies have therefore been communicated in which a wide spectrum of robust non-Newtonian models have been deployed. Relevant investigations include Hayat et al. [11] who deployed a Stokes polar fluid model to analyze non-Newtonian nanofluid squeeze films with couple stress effects. Hayat *et al.* [12] further implemented the Reiner-Rivlin second grade viscoelastic model for sensor squeezing dynamics to include stress relaxation effects. Bég *et al.* [13] deployed Eringen's micropolar rheological model to consider bionic squeezing flows in prosthetic dual plate systems with wall suction and injection effects. Other non-Newtonian models which have been deployed in squeezing regimes include the Bingham viscoplastic model [14] and the Ostwald-deWaele power-law nanofluid model [15]. An alternative and equally popular model for simulating squeeze film rheology is the *Carreau viscoelastic model*. This is a relatively simple but accurate model which allows the simulation of power-law rheological behaviour at high shear rates. Both pseudoplastic (shear-thinning) and dilatant (shear-thickening) behaviour can be analyzed depending on the rheological power-law index. The Carreau model is also easily accommodated into the framework of the Navier-Stokes equations. Experimental and numerical investigations of the squeezing motion of Carreau liquid in impact dynamics of a solid sphere was studied by Uddin *et al.* [16].

The emergence of increasingly functional lubricants in recent years has popularized magneto-tribology. Many new exciting "smart" fluids have been developed which feature embedded responsiveness to external agents including magnetic fields, electrical fields, light, pressure, acoustics etc. In sensor designs magnetohydrodynamic films [17] have permitted greater resolution and controllability of sensor designs [18]. To simulate the flow of magnetic fluids, the science of electromagnetics must be combined with viscous fluid mechanics. This is known as magnetohydrodynamics (MHD) and involves the modification of Navier-Stokes and non-Newtonian flow models with electromagnetic body forces based on the Maxwell equations [19]. The fundamental approach for simulating MHD squeeze films, for Newtonian liquids, was established by Kuzma [20]. Subsequently many diverse studies of MHD squeezing dynamics have been reported. Bhattacharyya and Pal [21] considered rotational effects in magnetic film squeezing flow. Umavathi *et al. [*22] used MATLAB quadrature and perturbation methods to compute the time-dependent squeezing flow of a magnetic nanofluid with mixed wall boundary conditions. Bég *et al.* [23] used the Liao homotopy analysis method to derive power-series solutions for magnetized micropolar squeezing film under an axial magnetic field at low magnetic Reynolds numbers. Bég *et al.* [24] used the Adomian decomposition method (ADM) to load capacity, disk torque and radial and azimuthal magnetic induction fields in hydromagnetic squeezing Newtonian flow between two electrically insulated disks. Shamshuddin *et al.* [25] used the method of variation of parameters (VPM) to study the effects of homogenous chemical reaction and micro-organism doping in magnetized squeezing flow. Non-Newtonian magnetic squeezing flows have also been studied in recent years. Khan *et al.* [26] applied the Casson viscoplastic model and homotopy perturbation method (HPM) to study unsteady hydromagnetic squeezing flow, noting a significant difference in plate friction factors for squeezing or separating plates and strong damping in the flow with high magnetic body force. Salahuddin *et al.* [27] employed a Runge–Kutta–Fehlberg method to compute the magnetic squeezing flow of Carreau-Yasuda fluid in a sensor system, noting that the flow is strongly decelerated with greater rheological power-law index, higher Hartmann number and greater Weissenberg number. While experimental studies of magnetized squeezing flows in micro-cantilevers have also been presented by for example, Datkos *et al.* [28] (using gold coatings on the sensor surfaces) and Lavrik *et al*. [29] (with gold nanocoatings and rheological lubricants), mathematical and numerical studies of magnetized Carreau squeezing flows have not yet received attention in the literature. Some important studies relating to heat transfer in magnetized sensor squeezing flows have however been reported and include the work of Khaled and Vafai [30] who considered wall permeability effects and computed Nusselt numbers over a range of magnetic field strengths. Usha and Naduvinamani [31] presented simulations on hydromagnetic squeezing flow of a time-dependent Prandtl-Eyring non-Newtonian liquid in a parallel plate sensor geometry. They showed that increasing magnetic parameter accelerates the flow and cools the lubricant. Higher wall (plate) permeable velocity parameter was also shown to reduce temperature magnitudes.

Non-Newtonian lubricants are known to exhibit viscous dissipation effects even at very low Reynolds numbers [32]. This involves the conversion of kinetic energy into thermal energy. Substantial viscous heating has been computed in thermal flows of viscoelastic fluids [33] and power-law liquids [34]. In the presence of magnetic fields, Ohmic dissipation or Joule heating [35] may also arise. This manifests in the loss of electric energy when an electric current is flowing through a real fluid, due to conversion into heat. It is therefore an important phenomenon in real MHD systems where viscous fluids are utilized. Several researchers have considered viscous and/or Joule heating effects in MHD squeezing flows including Khan *et al.* [36] who examined viscous dissipation in the squeezing flow of Cu-water and Cu-kerosene nanofluids. Duwairi *et al.* [37] studied squeezing flow and heat transfer in Newtonian fluids with viscous heating. Joule heating effects in magnetohydrodynamic non-Newtonian (micropolar) squeezing flow of alumina (Al_2O_3), titania (TiO_2) or magnetite (Fe_3O_4)-water nanofluids was studied by Sastry *et al.* [38]. Further studies include Mishra *et al.* [39] who simulated the combined effects of viscous and Joule dissipation in electromagnetic actuator squeezing flow with the additional effects of thermal relaxation and radiative flux. Zubair *et al.* [40] investigated the magnetized squeezing flow of an electro-conductive viscoplastic nanofluid between rotating plates with Joule heating, viscous heating and entropy generation.

Magodora et al. [41] studied the influence of activation energy and Brownian motion on the flow of time-independent two-dimensional viscous incompressible gold-water nanofluid fluid over a rotating disk under chemical reaction effect. It is recorded from their analysis that, rising activation energy suppressed the thermal field. Almakki et al. [42] discussed the effect of magnetic and viscous dissipation on double diffusion flow of convective nanofluid under entropy generation impact. It is noticed from their investigation that, the rising radiation number raises the thermal profile. Almakki et al. [43] investigated the impact of Brownian motion and stratification on the non-Newtonian flow of micropolar nano fluid over a stretching surface under the influence of entropy generation process. It is recorded from their analysis that, the rising thermophoresis parameter enhances the temperature profile. Dhlamini et al. [44] described the influence of activation energy and entropy generation on the viscous incompressible two-dimensional flow of nanofluid over a stretching sheet under the impact of Brownian motion and thermophoresis effect. Sithole et al. [45] discussed the impact of magnetic field on the time-dependent micropolar nanofluid over a stretching surface under the action of homogeneous-heterogeneous chemical reaction via Bivariate Spectral Local Linearization Method. It is observed from their investigation that, the rising Schmidt number magnifies the concentration distribution in the flow regime.

Variable thermophysical properties may also arise in thermal squeezing flow regimes. An important characteristic is thermal conductivity variation which can dramatically influence temperature distributions at the walls and also durability of the materials deployed in sensor microplates. Khan *et al.* [46] simulated the effect of thermal conductivity variation on thermal squeezing flow of a Carreau fluid in between sensor plate surfaces. Kumar *et al.* [47] considered the transient heat transfer and squeezing flow of a tangent hyperbolic fluid in sensor parallel plate geometry with variable thermal conductivity. Usha *et al.* [48] recently used a Runge-Kutta numerical scheme to compute the thermal conductivity variation effects on magnetic squeezing flow and heat transfer in a Williamson non-Newtonian fluid, showing that temperatures are suppressed with greater thermal conductivity parameter and Nusselt number is elevated with higher magnetic parameter, whereas temperatures are enhanced with higher Weissenberg parameter.

Inspection of the literature has revealed that thus far the *collective effects of variable thermal conductivity, viscous and Joule heating in the unsteady boundary layer flow of a magnetized Carreau liquid over a micro-cantilever sensor system, suspended in a squeezing plate regime, has not been examined*. This is the focus of the present study which aims to generalize previous studies and provide a more robust multi-physical analysis of relevance to biomedical designs for pathogen and disease detection. The governing conservation equations for unsteady magnetic Carreau squeezing flow and heat transfer are rendered dimensionless and self-similar via appropriate scaling transformations. The emerging nonlinear coupled boundary value problem is then solved with an efficient numerical method (Runge-Kutta 4th order shooting technique RK4 in MATLAB software). Validation of solutions with earlier simpler models over a range of Prandtl numbers and squeezing parameter values is included. Comprehensive analysis and extensive graphical visualization is included in order to quantify the thermal and hydrodynamic behaviour for the influence of key emerging parameters.

2. CARREAU NON-NEWTONIAN FLUID MODEL

The classical mathematical relations governing the flow of incompressible Carreau liquid are the continuity, momentum and temperature equations. These may be stated as follows [16, 46]:

$$\operatorname{div}\mathbf{V} = 0 \tag{1}$$

$$\rho\left(\frac{d\mathbf{V}}{dt}\right) = \operatorname{div}\boldsymbol{\tau} \tag{2}$$

$$\rho c_p\left(\frac{dT}{dt}\right) = \boldsymbol{\tau}.\mathbf{L} - \operatorname{div}\mathbf{q} \tag{3}$$

Here, $\mathbf{V}$ is the velocity vector, ρ is the density of the Carreau liquid, T is liquid temperature, c_p specific heat, $\mathbf{q} = -k$ grad T is Fourier thermal flux and k is fluid conductivity, $\mathbf{L} = \boldsymbol{\nabla}\mathbf{V}$ and $\frac{d}{dt}$ represents total time derivative. Further, the Cauchy stress tensor $(\boldsymbol{\tau})$ for a Carreau fluid flow is taken as below:

$$\boldsymbol{\tau} = -p\boldsymbol{I} + \zeta\mathbf{A_1} \tag{4}$$

The value of ξ in Eq. (1) is taken as below:

$$\zeta = \zeta_\infty + (\zeta_0 - \zeta_\infty)(1 + (\Omega\lambda)^2)^{\frac{n-1}{2}} \tag{5}$$

In Eqns. (1) and (2), p is pressure, $\boldsymbol{I}$ is identity tensor, ζ_0 viscosity at zero rate of shear, ζ_∞ viscosity at infinite rate of shear, Ω is time-constant, n power-law index (n predicts the slope of $(\zeta - \zeta_\infty/\zeta_0 - \zeta_\infty)$ in the rheological power-law region), $\mathbf{A_1}$ is 1st Rivlin–Ericksen tensor. Also λ is the *shear rate* which is defined as follows:

$$\lambda = \sqrt{\frac{1}{2}\sum_j \lambda_{ij}\sum_j \lambda_{ji}} = \sqrt{\frac{1}{2}\boldsymbol{\Pi}} = \sqrt{\frac{1}{2}tr(\mathbf{A}_1^2)} \tag{6}$$

Here $\boldsymbol{\Pi}$ is the 2nd invariant strain rate tensor and $\mathbf{A_1}$ is defined as follows:

$$\mathbf{A_1} = (\text{grad}\,\mathbf{V}) + (\text{grad}\,\mathbf{V})^{\mathrm{t}} \tag{7}$$

In the regime to be studied (squeezing micro-cantilever flow) it is realistic to consider the case in which $\zeta_0 \gg \zeta_\infty$ [30]. Therefore, adopting $\zeta_\infty = 0$ in the present study, Eqn. (1) reduces to following form:

$$\boldsymbol{\tau} = -p\boldsymbol{I} + \zeta_0[1 + (\Omega\lambda)^2]^{\frac{n-1}{2}} \tag{8}$$

Thus, based on the Carreau fluid model, the power-law rheological index ranges are $0 < n < 1$ for *pseudoplastic or shear thinning fluids* and $n > 1$ for *dilatant or shear thickening fluids*. Since two-dimensional flow with heat transfer is considered in the squeezing lubrication problem, the velocity and thermal components are assumed to be of the form:

$$\mathbf{V} = [u(x,y), v(x,y), 0] \text{ and } T = T(x,y) \tag{9}$$

Here u, v designate the velocity components along the x and y directions, respectively. Implementing Eqns. (7) and (9) into Eq. (6), then the shear rate, λ is given by.

$$\lambda = \left[4\left(\frac{\partial u}{\partial x}\right)^2 + \left(\frac{\partial u}{\partial y} + \frac{\partial v}{\partial x}\right)^2 \right]^{1/2} \tag{10}$$

3. MAGNETOHYDRODYNAMIC DISSIPATIVE CARREAU SQUEEZE FILM MODEL

Unsteady 2-dimensional magnetized incompressible laminar non-Newtonian electrically conducting Carreau fluid boundary layer flow is considered over a micro-cantilever suspended in a parallel plate squeezing regime. A vertical static magnetic field is applied. Viscous dissipation and Joule heating are incorporated in the analysis as is variable thermal conductivity of the magnetic Carreau liquid. Free stream effects are also included. However magnetic Reynolds number is sufficiently small to neglect magnetic induction effects. The flow geometry depicted in **Fig. 1** illustrates the physical model (closed squeezing channel) with annotation.

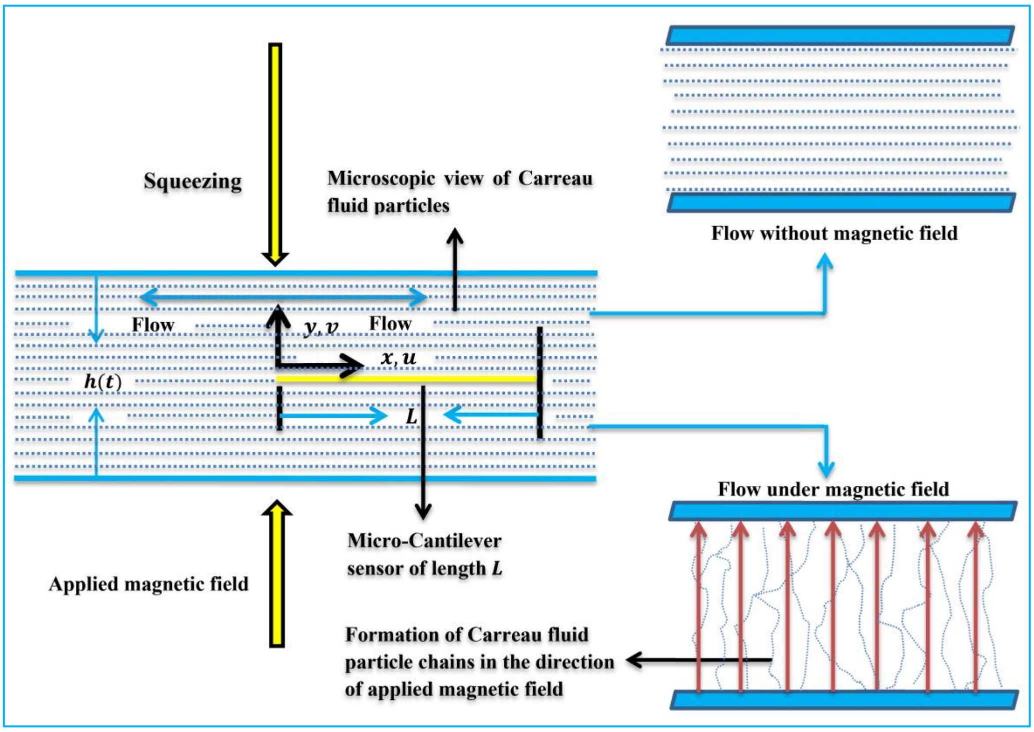

Fig. 1: Micro-cantilever magnetic Carreau fluid squeeze film geometry

The transient vertical depth $h(t)$ i. e. gap between the plates, of the closed squeezing channel varies from 0 to h and this is considerably larger than the boundary layer thickness at the wall. Also, a microcantilever floating sensor of length L is suspended between plates. The upper plate of the channel is fixed, whereas the top surface is mobile in the vertical direction (*descending towards the lower plate for squeezing and ascending away from the lower plate for separating*). It is known that the squeezing phenomena start at the tip of the sensor sheet. The Carreau liquid movement about the floating sensor is produced due to the outside ambient velocity $U(x,t)$ and the normally applied magnetic field B_o. In addition to this, in the mathematical model based on the adopted $x-y$-coordinate system, the x-direction is the dominant flow path. Thus, with the above considerations and incorporating the appropriate terms from the Carreau non-Newtonian model described in Section 2, the fundamental conservation equations for magnetohydrodynamic (MHD) squeezing flow of Carreau liquid between the plates (sensor geometry) and external to the micro-cantilever (for which a *free stream momentum equation* is needed) can be shown, by extending earlier models in [31-38], to take the form.

Continuity Equation:

$$\frac{\partial u}{\partial x}+\frac{\partial v}{\partial y}=0 \tag{11}$$

MHD-modified Momentum Equation:

$$\frac{\partial u}{\partial t}+u\frac{\partial u}{\partial x}+v\frac{\partial u}{\partial y}=-\frac{1}{\rho}\left(\frac{\partial p}{\partial x}\right)-\left(\frac{\sigma B_o^2}{\rho}\right)u+\nu\left(\frac{\partial^2 u}{\partial y^2}+3\frac{(n-1)}{2}\Omega^2\left(\frac{\partial u}{\partial y}\right)^2\frac{\partial^2 u}{\partial y^2}\right) \tag{12}$$

Free Stream Equation:

$$\frac{\partial U}{\partial t}+U\frac{\partial U}{\partial x}=-\frac{1}{\rho}\left(\frac{\partial p}{\partial x}\right)-\left(\frac{\sigma B_o^2}{\rho}\right)U \tag{13}$$

Thermal Energy Equation:

$$\frac{\partial T}{\partial t}+u\frac{\partial T}{\partial x}+v\frac{\partial T}{\partial y}=\frac{\partial}{\partial y}\left(\alpha(T)\frac{\partial T}{\partial y}\right)+\frac{\nu}{C_p}\left(\frac{\partial u}{\partial y}\right)^2+\left(\frac{\sigma B_o^2}{\rho C_p}\right)u^2 \tag{14}$$

In Eqs. (11)-(14), u, v, denote the velocity components in x, y directions, U is ambient magnetic fluid velocity in x-direction, T is liquid temperature, t is time, ρ be liquid density, Ω is a temporal constraint parameter, $\alpha(T)$ is the variable thermal conductivity, ν is kinematic viscosity of the magnetic Carreau liquid, B_o is the magnetic field strength. The penultimate term in Eqn. (14) represents the *viscous dissipation* and the ultimate term on the right-hand side is the *Joule dissipation* (Ohmic heating) term. Further, Eqs. (12) and (14) obeys all the essential conditions inside the squeezing flow zone considered in the current investigation. Also, Eq. (13) describes the external ambient liquid motion ($u \to U, v \to 0$) which is presumed to be uniform and inviscid. Additionally, any induced error due to the above assumptions are resolved by considering a small floating sensor length with response to channel height, following Khaled and Vafai [30]. With all these predictions, using Eqns. (12) and (13) the pressure term is removed, and the required momentum conservation equation is obtained as below.

$$\frac{\partial u}{\partial t}+u\frac{\partial u}{\partial x}+v\frac{\partial u}{\partial y}=\frac{\partial U}{\partial t}+U\frac{\partial U}{\partial x}+\frac{\sigma B_o^2}{\rho}(U-u)+\nu\left(\frac{\partial^2 u}{\partial y^2}+3\frac{(n-1)}{2}\Omega^2\left(\frac{\partial u}{\partial y}\right)^2\frac{\partial^2 u}{\partial y^2}\right) \tag{15}$$

To solve the coupled momentum and thermal energy Eqns. (14) and (15), the following velocity and thermal boundary conditions are prescribed [46].

$$\left.\begin{array}{ll} \left.\begin{array}{c} u(x,0,t)=0, v(x,0,t)=v_o(t), \\ -k\frac{\partial T(x,0,t)}{\partial y}=q(x) \end{array}\right\} & \text{at } y=0 \\ \left.\begin{array}{c} u(x,\infty,t)\to U(x,t), \\ T(x,\infty,t)\to T_\infty \end{array}\right\} & \text{as } y\to\infty \end{array}\right\} \tag{16}$$

In Eqn. (16), $U(x,t)$and T_∞ are free stream velocity and free stream temperature, $q(x)$ is the thermal wall flux. Also, in current analysis $\alpha(T)$ denotes the variable thermal conductivity and is articulated as $\alpha(T)=\alpha_\infty(1+\epsilon\theta)$, in which ϵ is a small number and represents the *thermal conductivity variation parameter*. For the case where the sensor sheet surface is a function of wall thermal flux $q(x)$ may be varied. Also $v_o(t)$ depicts the wall suction/injection velocity at the sensor wall when the surface is assumed to be permeable and permits lateral mass influx.

To facilitate numerical solutions of the defined nonlinear coupled boundary value problem, we invoke suitable similarity variables. By virtue of these scaling transformations the 2-dimensional unsteady magnetized Carreau fluid conservation boundary layer flow Eqns. (14) and (15) and also the boundary conditions defined by Eqn. (16) are rendered into a *nonlinear ordinary differential boundary value problem*. Hence introducing the similarity transformations:

$$\left.\begin{array}{ll} U = ax, \;\; u = axf'(\eta), & \eta = y\sqrt{\frac{a}{\nu}}, \\ \psi = f(\eta)x\sqrt{a\nu}, & a = \frac{1}{s+bt}, \\ v = -f(\eta)\sqrt{a\nu}, & \theta(\eta) = \frac{T-T_\infty}{\frac{q_o x}{k}\sqrt{\frac{\nu}{a}}}, \\ v_o(t) = v_i\sqrt{a}, & q(x) = q_o x \end{array}\right\} \tag{17}$$

In Eqn. (17), s indicates an arbitrary number, a is the squeezing flow strength parameter (which is a function of the plate gap separation distance parameter, *b and time*, *t*), q_o is a wall thermal flux, $q(x) = q_o x$ and k is magnetic Carreau fluid thermal conductivity. The movement of the plate gap (vertical length) obeys the expression $h(t) = \frac{1}{(s+bt)^{1/b}}$ with $b\ (\mathit{squeezing\ flow\ index\ i.e.plate\ gap\ parameter}) > 0$ and $h(t) = h_o e^{-st}$ with $b = 0$, h_o is fixed i. e. the plates are a constrained distance apart [32]. Further, the flow field f_o is amplified with diminishing time t under $b > 0$,. This is due to the flow field being enhanced with decaying t inside the squeezing flow domain. The dimensional stream function, ψ, satisfies the continuity (mass conservation) by virtue of the Cauchy-Riemann equations, $u = \frac{\partial\psi}{\partial y}$ and $v = -\frac{\partial\psi}{\partial x}$. Introduction of Eqn. (17) into Eqns. (14)-(15) leads to the following system of dimensionless coupled, nonlinear ordinary differential equations representing the flow with respect to the non-dimensional transverse coordinate, η:

$$\begin{gathered} f'''(\eta) + \left(f(\eta) + \frac{b\eta}{2}\right) f''(\eta) - \left(f'(\eta)\right)^2 + \\ \frac{3}{2}(n-1)We^2\left(f''(\eta)\right)^2 f'''(\eta) + \\ M\left(1 - f'(\eta)\right) + b(f'(\eta) - 1) + 1 = 0 \end{gathered} \tag{18}$$

$$\begin{gathered} \left(1 + \epsilon\theta(\eta)\right)\theta''(\eta) + Pr\left(f(\eta) + \frac{b\eta}{2}\right)\theta'(\eta) \\ -Pr\left(f'(\eta) + \frac{b}{2}\right)\theta(\eta) + \epsilon\left(\theta'(\eta)\right)^2 + \\ PrEc\left(f''(\eta)\right)^2 + PrEcM\left(f'(\eta)\right)^2 = 0 \end{gathered} \tag{19}$$

Furthermore, via the transformations in Eqn. (17), the boundary conditions (16) emerge as the following dimensionless conditions:

$$\left.\begin{array}{l} f(0) = -f_o, f'(0) = 0, \theta'(0) = -1, at\ \eta = 0 \\ f'(\infty) = 1, \quad \theta(\infty) = 0 \quad at \quad \eta = \infty \end{array}\right\} \tag{20}$$

In Eqns. (18)-(20), the superscript "prime" depicts the ordinary derivative with respect to η. The magnetic, rheological and thermophysical parameters featuring in Eqns. (18) and (19) which are the problem control parameters regulating the flow of magnetized Carreau fluid over the floating surface are defined as $M = \frac{\sigma B_o^2}{\rho a}$ (Magnetic body force number), $We = ax\Omega\sqrt{\frac{a}{\nu}}$ (Weissenberg viscoelastic number), b (squeezing flow index), n (Carreau rheological power law index), $f_o = \frac{v_i}{\sqrt{\nu}}$ (permeable velocity parameter i.e. wall transpiration velocity), $Pr = \frac{\nu}{\alpha}$ (Prandtl number), ϵ (thermal conductivity parameter) and $Ec = \frac{U^2}{C_p\left(\frac{q_o x}{k}\right)\sqrt{\frac{\nu}{a}}}$ (Eckert dissipation number). In the energy Eqn. (19) the penultimate term is the *viscous heating term,* and the final term is the *Joule dissipation term (magnetic Ohmic heating)*.

A number of important wall gradients can also be defined based on the primitive variables featured in the Eqns. (18) and (19). These are *skin-friction (wall shear stress)* and *heat transfer rate* at the wall which furnish important information on momentum and thermal transport at the boundary. Skin friction coefficient and local Nusselt number (temperature gradient at the wall) are for the present problem defined as follows:

$$C_f = \frac{2\tau_w}{\rho U^2} \tag{21}$$

$$Nu_x = \frac{x q_w}{q_o x\sqrt{\frac{\nu}{a}}} \tag{22}$$

Here the shear stress τ_w and wall heat flux q_w in Eqs. (21) and (22) are defined as below:

$$\left.\begin{aligned} \tau_w &= \left(\frac{\partial u}{\partial y} + \Omega^2\left(\frac{n-1}{2}\right)\left(\frac{\partial u}{\partial y}\right)^3\right)_{y=0} \\ q_w &= -k\left(\frac{\partial T}{\partial y}\right)_{y=0} \end{aligned}\right\} \tag{23}$$

Finally, involving the dimensionless transformations defined in Eqn. (17), non-dimensional skin friction coefficient and Nusselt number assume the form:

$$C_f\sqrt{Re_x} = \left[f''(\eta) + We\left(\frac{n-1}{2}\right)\left(f''(\eta)\right)^3\right]_{\eta=0} \tag{24}$$

$$Nu_x\sqrt{Re_x} = -[\theta'(\eta)]_{\eta=0} \tag{25}$$

Eqns. (24) and (25) provide the required momentum and thermal characteristics at the boundaries (plates). In both expressions, $Re_x = x\sqrt{\frac{a}{\nu}}$ is the local Reynolds number.

4. NUMERICAL SOLUTION METHODOLOGY

The dimensionless conservation equations and associated boundary conditions describing magnetized transient Carreau fluid boundary layer flow about a floating sensor sheet (micro-cantilever) with variable thermal conductivity and viscous and Joule dissipation effects and engulfing squeezing have been derived in the previous section. The strongly *nonlinear* nature of the momentum and energy ordinary differential equations (ODEs) i. e. Eqns. (18), (19) render them difficult to solve analytically. A computational approach is therefore adopted, namely the robust Runge-Kutta 4th order (RK-4) shooting scheme. This method has proved very versatile and has been implemented in many magneto-thermophysical flow studies including Usha *et al*. [48], Basha [49], Bég [50] and Usha *et al.* [51]. This method reduces the multi-degree, multi-order nonlinear ODEs (18)-(19) into a group of 1st-order ODEs. Additionally, an attention is given to select the boundary layer domain and $\eta = 3$ is adopted as the boundary since this affords a location sufficiently far away from the free stream (edge of the viscous and thermal boundary layers) which is equivalent to η_∞. However, the choice $\eta = 3$ is reasonable to predict the boundary layer behaviour of existing parameters and is tabulated and discussed in the next section. With all these specifications, the 1st -order ODEs associated with Eqn. (18) to be solved with RK-4 become:

$$\left.\begin{aligned} f(\eta) &= \Gamma_1 \\ f'(\eta) &= \Gamma_1' = \Gamma_2 \\ f''(\eta) &= \Gamma_2' = \Gamma_3 \\ f'''(\eta) &= \Gamma_3' = \Gamma_4 \end{aligned}\right\} \tag{26}$$

In Eqn. (26) the expression for Γ_4 is derived from Eqn. (17) and is defined as:

$$\Gamma_4 = \left(\frac{1}{1+\frac{3}{2}(n-1)We\Gamma_3^2}\right)\left[\Gamma_2^2 - \left(\Gamma_1 + \frac{b}{2}\eta\right)\Gamma_3 + b(1-\Gamma_2) + M(\Gamma_2 - 1) - 1\right] \tag{27}$$

Further, the group of 1st order ODEs corresponding to Eqn. (19) are summarized below:

$$\left.\begin{aligned} \theta'(\eta) &= \Gamma_5' = \Gamma_6 \\ \theta''(\eta) &= \Gamma_6' = \Gamma_7 \end{aligned}\right\} \tag{28}$$

In Eqn. (27) the the expression for Γ_7 is derived from Eqn. (18):

$$\Gamma_7 = \left(\frac{1}{1+\varepsilon\,\Gamma_5}\right)\left[Pr\left(\Gamma_2 + \frac{b}{2}\right)\Gamma_5 - Pr\left(\Gamma_1 + \frac{b}{2}\eta\right)\Gamma_6 - \varepsilon{\Gamma_6}^2 - PrEc\left({\Gamma_3}^2 + M{\Gamma_2}^2\right)\right] \tag{29}$$

Also, the applicable boundary conditions i. e. Eqn. (20) are described below:

$$\left.\begin{aligned} &\Gamma_1(\eta) = -f_o, \Gamma_2(\eta) = 0, \Gamma_6(\eta) = -1 \; at \; \eta = 0 \\ &\Gamma_2(\eta) = 1, \qquad \Gamma_5(\eta) = 0 \quad as \quad \eta = \infty \end{aligned}\right\} \tag{30}$$

While applying RK-4 technique to solve diminished Eqs. (26)-(29), five preliminary conditions are required. However according to Eqn. (30) only three preliminary conditions are available when $\eta = 0$ and remaining two required conditions are produced by setting $\Gamma_2(\eta) \to 1$, $\Gamma_5(\eta) \to 0$ as $\eta \to \infty$. Hence, this replacement is equivalent to $\Gamma_2(0) = \xi_1$, $\Gamma_5(0) = \xi_2$. Next, Newton-Raphson iteration is utilized to generate suitable values of ξ_1 and ξ_2 for the accounted control variables and free stream conditions inside the flow regime. Finally, the generated values of ξ_1 and ξ_2 are modified to obey the periphery conditions at $\eta \to \infty$. Consequently, the diminished IVP is resolved by employing RK- 4 scheme. Further, we have chosen 10^{-5} as the convergence criterion with $h' = 0.01$ as the numerical step length for simulations which are executed in the symbolic software, MATLAB.

5. MATLAB CODE VALIDATION

Accuracy of the present RK-4 MATLAB code is tested by validating current solutions with earlier computations reported by Khaled and Vafai [30] and Usha *et al.* [48] for various Prandtl numbers and squeezed flow index values, in the *case of constant thermal conductivity i. e.* $\varepsilon = 0$, *a solid wall* ($f_0=0$) *and absent magnetic field* ($M = 0$). The comparison is documented in **Table 1**.

Table 1. Simulated comparison results with Khaled and Vafai [30] and Usha *et al.* [48] for $\theta(0)$ with $M = f_o = \varepsilon = 0$.

Prandtl number (Pr)	Squeezed flow index (b)	Khaled and Vafai [30]	Usha *et al.* [48]	Present RK4 solutions
0.71	1.0	1.03228	1.032282821145898	1.032255
2.0		0.65412	0.654123423120187	0.654120
5.0		0.43561	0.435614607270683	0.435614
6.7		0.38182	0.381823375689146	0.381823
6.7	0.5	0.46313	0.463137508447626	0.463137
	1.0	0.38182	0.381823375689146	0.381823
	1.5	0.33084	0.330840498714310	0.330840
	2.0	0.29544	0.295440261684154	0.295440

Excellent correlation is achieved with the solutions of Khaled and Vafai [30] and Usha et al. [48] and this confirms high confidence in the accuracy of the present MATLAB RK4 code. It is also noteworthy that Table 1 shows that amplifying Prandtl and squeezed flow parameter values significantly decays temperatures i. e. cools the regime.

6. RESULTS AND DISCUSSION

Extensive computations have been performed with MATLAB RK4 to describe the influence of key parameters emerging in hydromagnetic thermal Carreau liquid flow over a sensor sheet on *velocity, temperature, skin-friction and heat transfer rates*. Parameters investigated include the magnetic number (M), rheological power-law index (n), permeable velocity i. e. wall transpiration (f_o), Weissenberg parameter (We), Eckert parameter (Ec), squeezing flow index number (b), Prandtl number (Pr) and thermal conductivity parameter (ε). All velocity and temperature plots are presented in **Figs. 3-14**. Furthermore, the influence of selected parameters on skin-friction and local Nusselt number are given in **Table 2** and also in **Figs. 15-18**. All data is extracted from [30], [47] and is physically viable for actual magnetic sensor squeezing flows.

Weissenberg number effect on velocity and temperature distributions

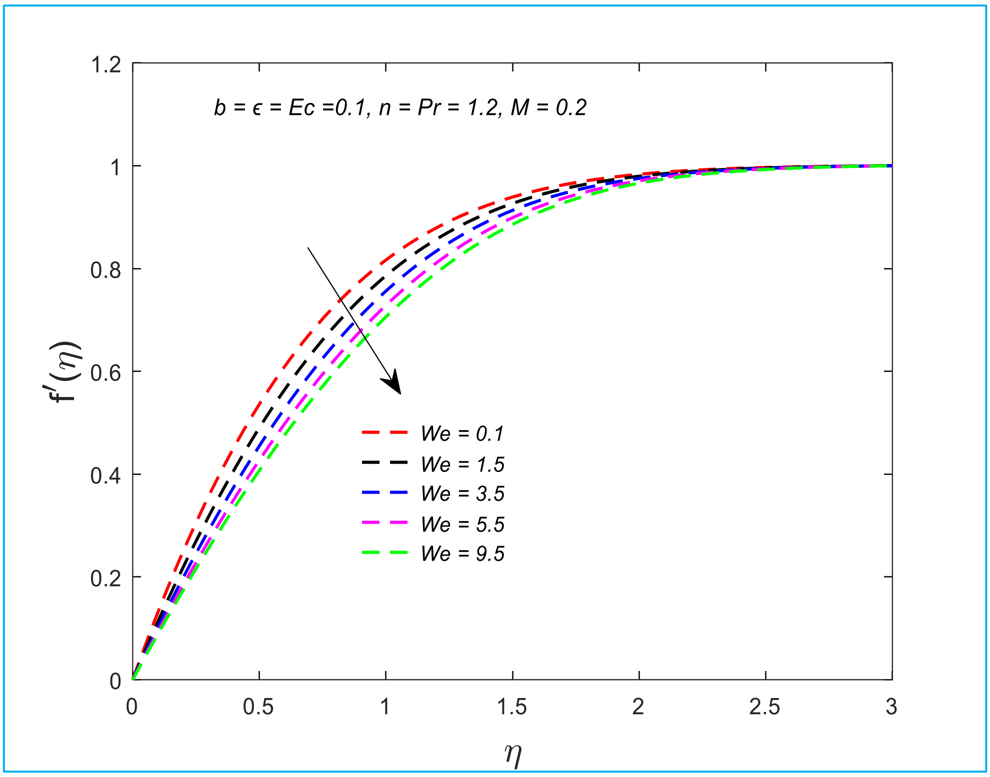

Fig. 2. Velocity evolution with Weissenberg number, We.

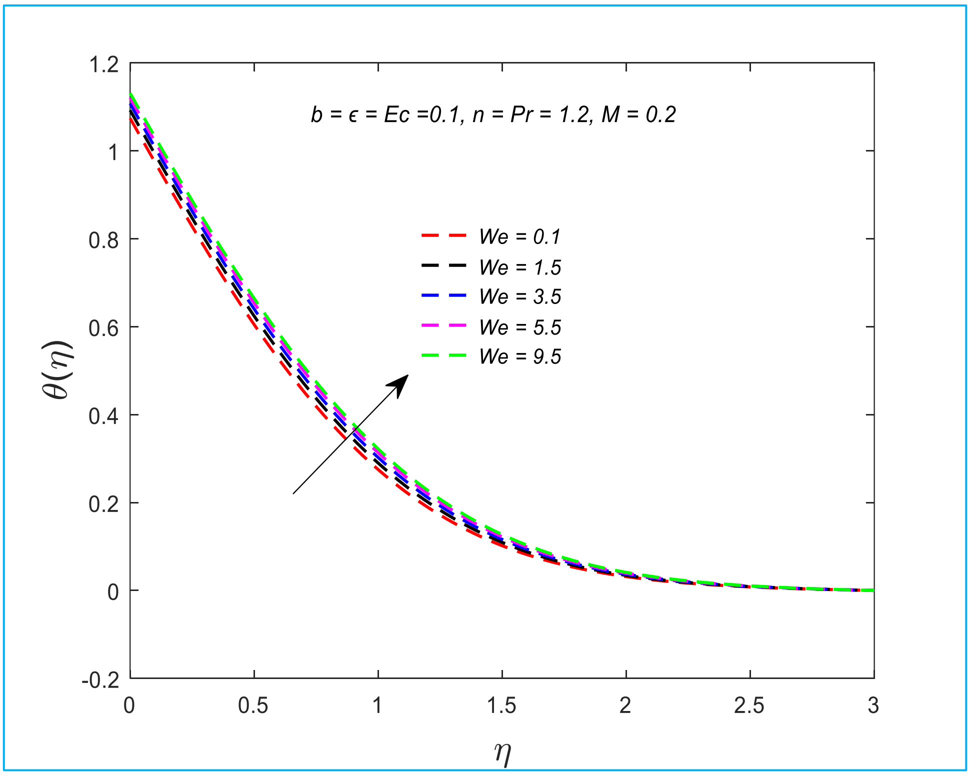

Fig. 3. Temperature distribution with Weissenberg number, We.

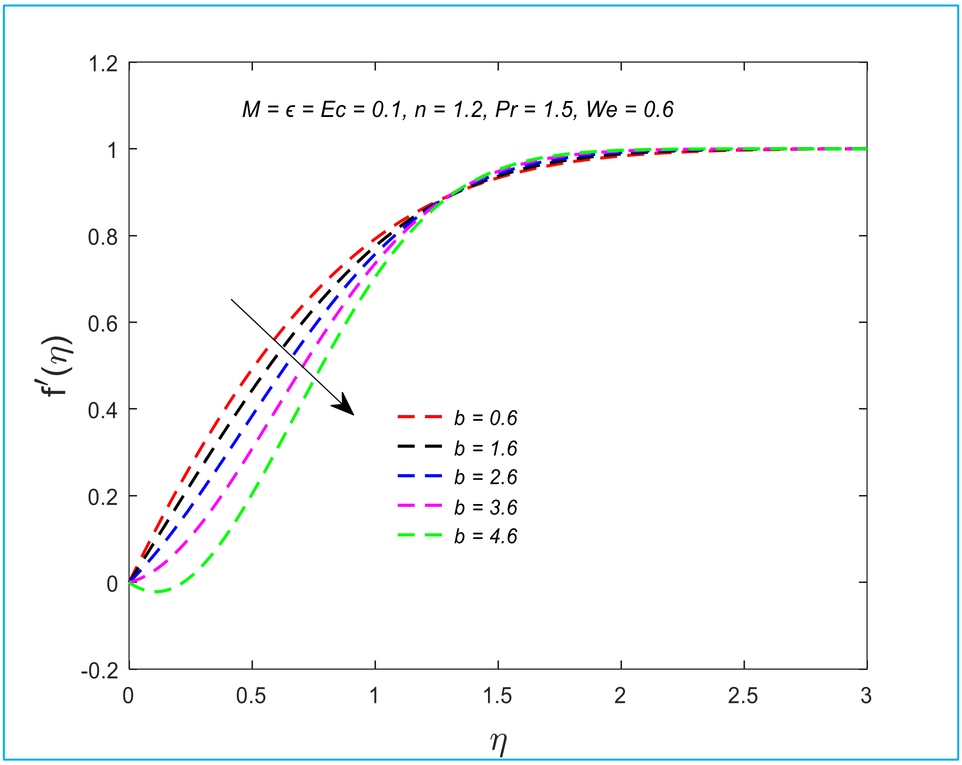

Fig. 4. Velocity evolution with squeezing index parameter, *b*.

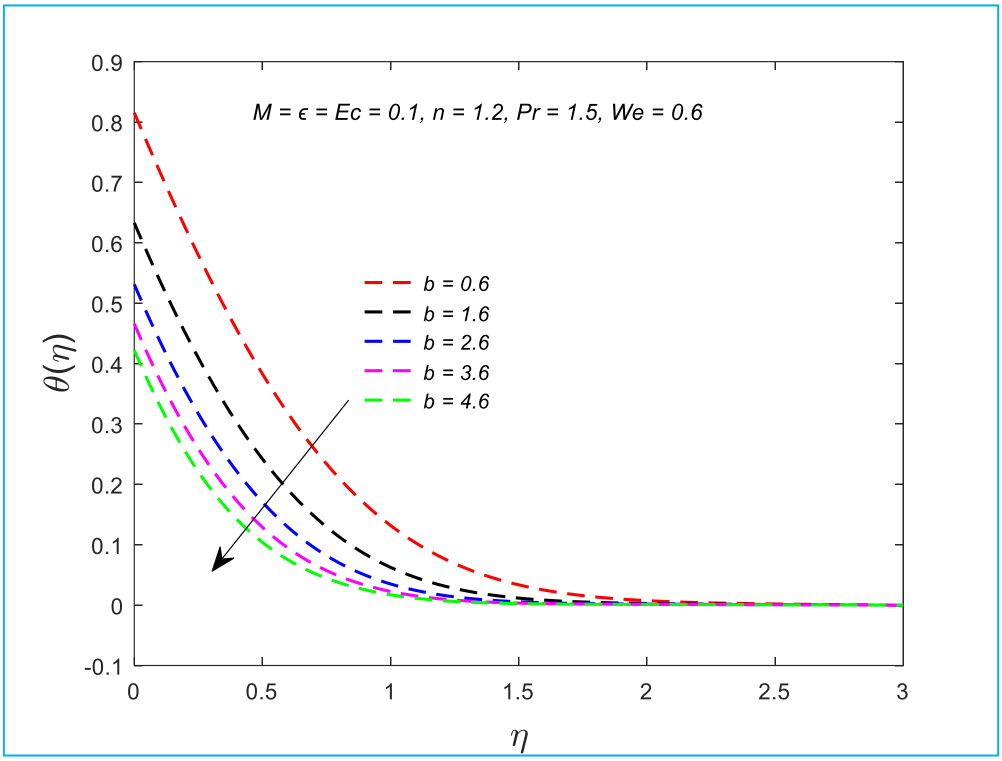

Fig. 5. Temperature distribution with squeezing index parameter, *b*.

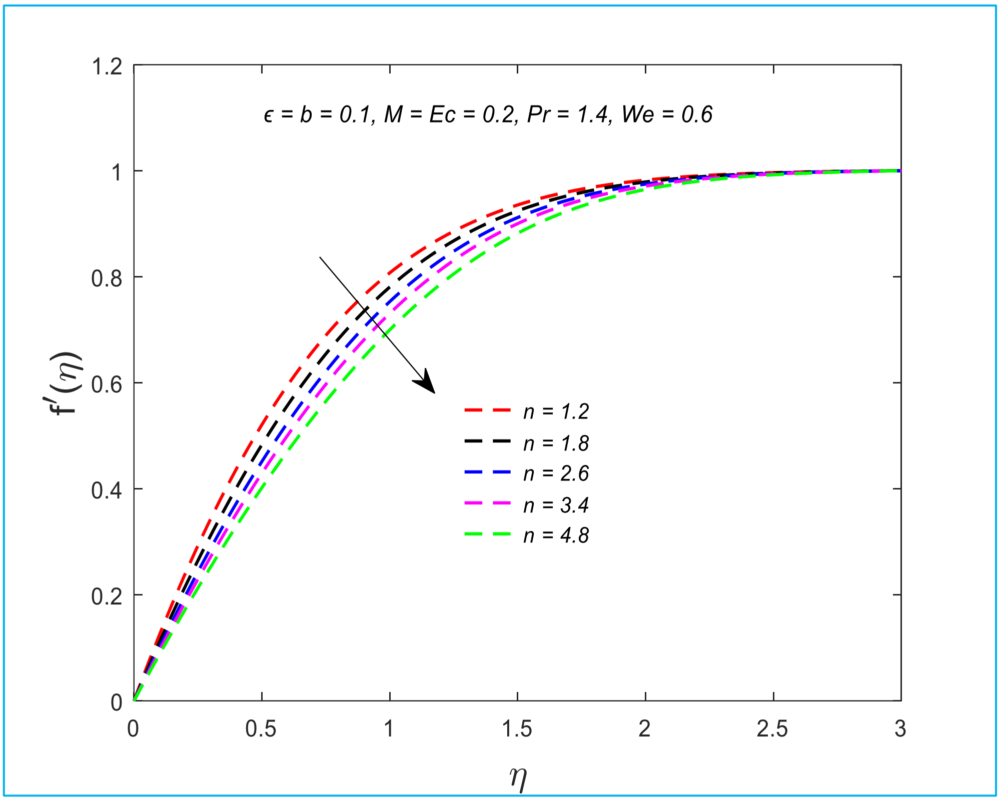

Fig. 6. Velocity evolution with Carreau rheological power-law index, n.

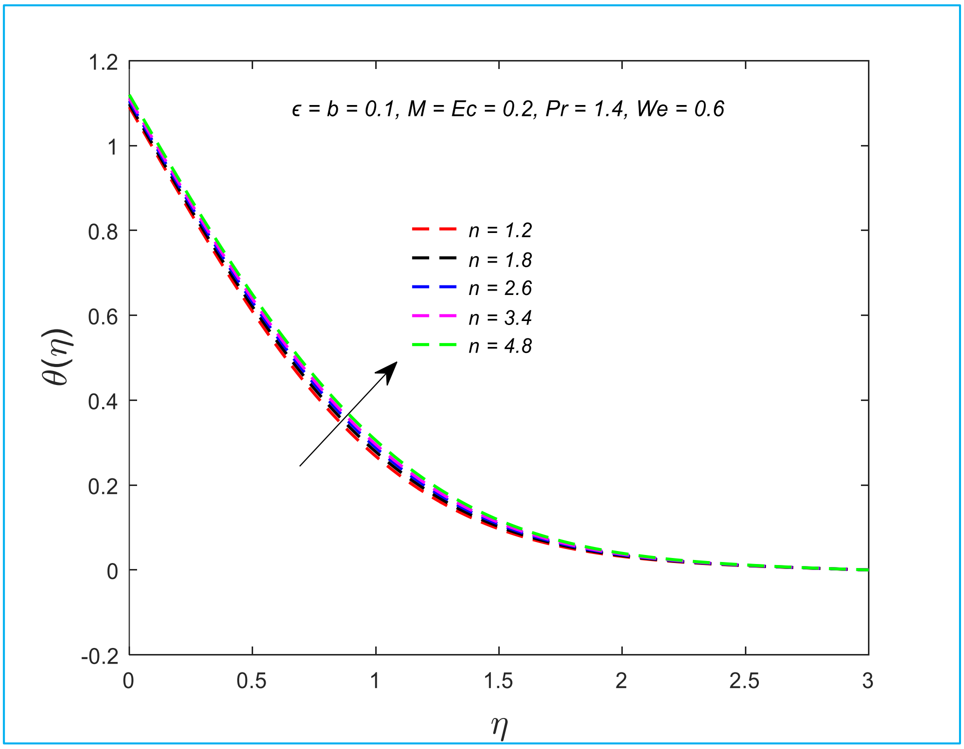

Fig. 7. Temperature distribution with Carreau rheological power-law index, n.

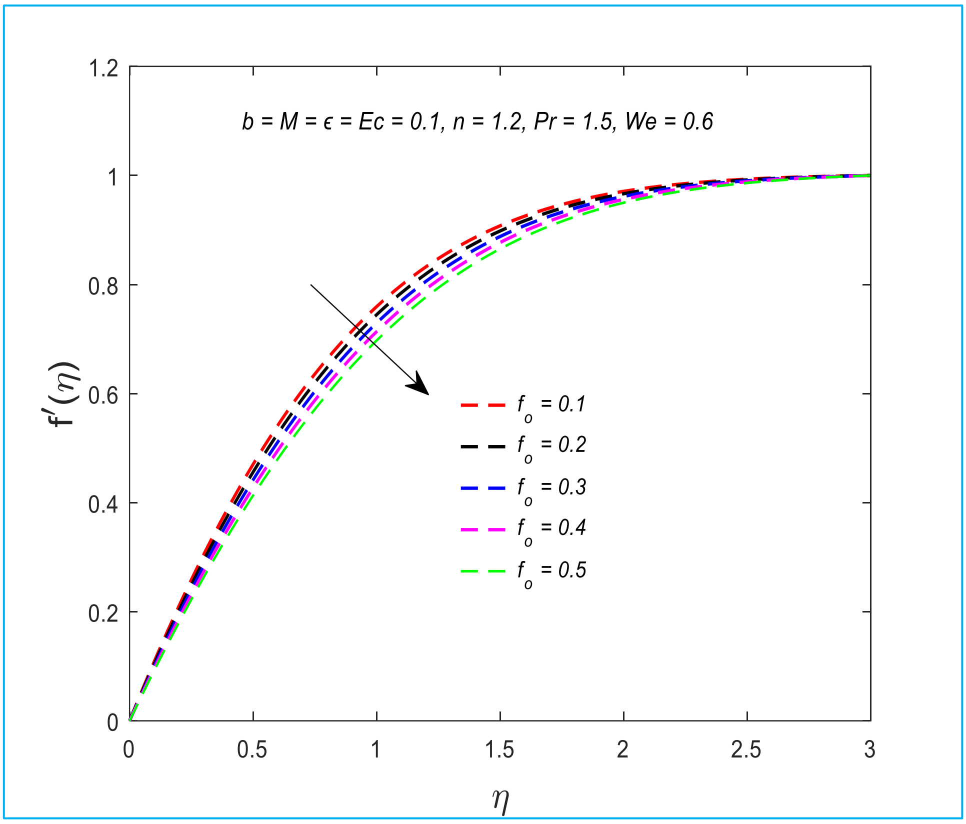

Fig. 8. Velocity evolution with permeable wall velocity, f_o.

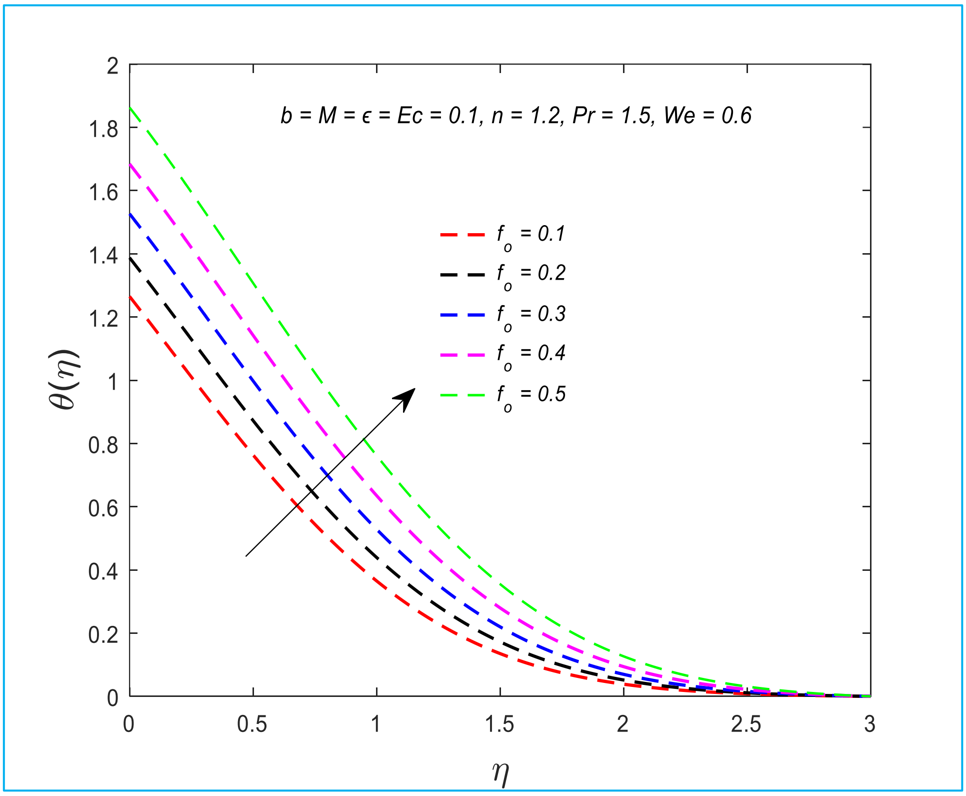

Fig. 9. Temperature distribution with permeable wall velocity, f_o.

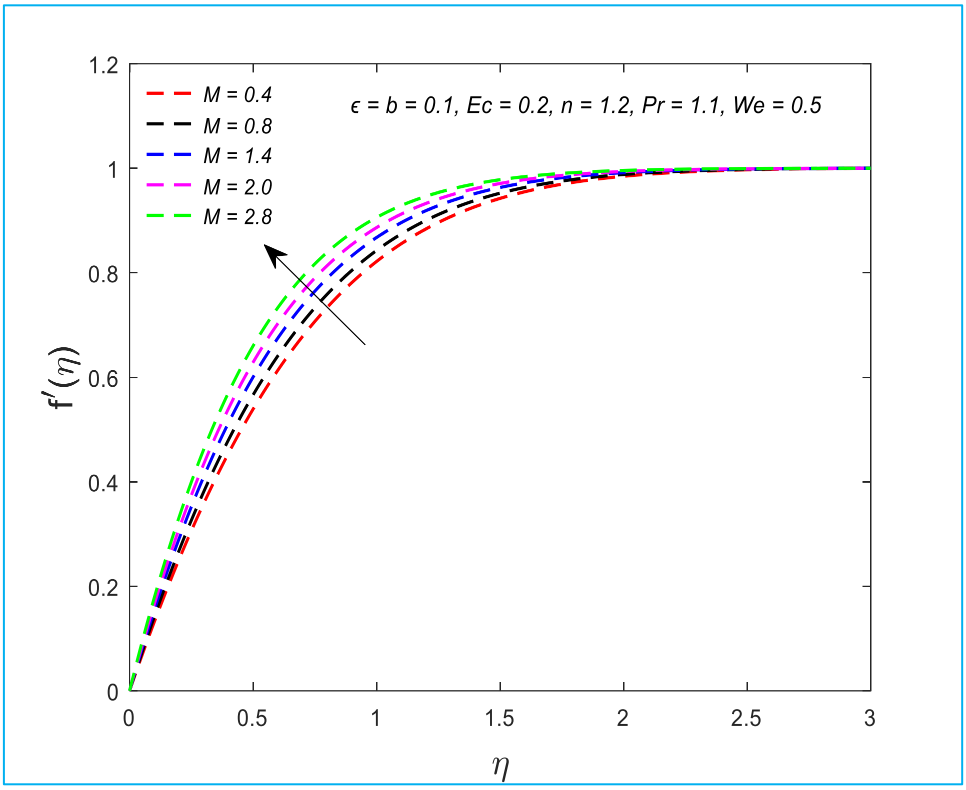

Fig. 10: Velocity profile with magnetic body force number, M.

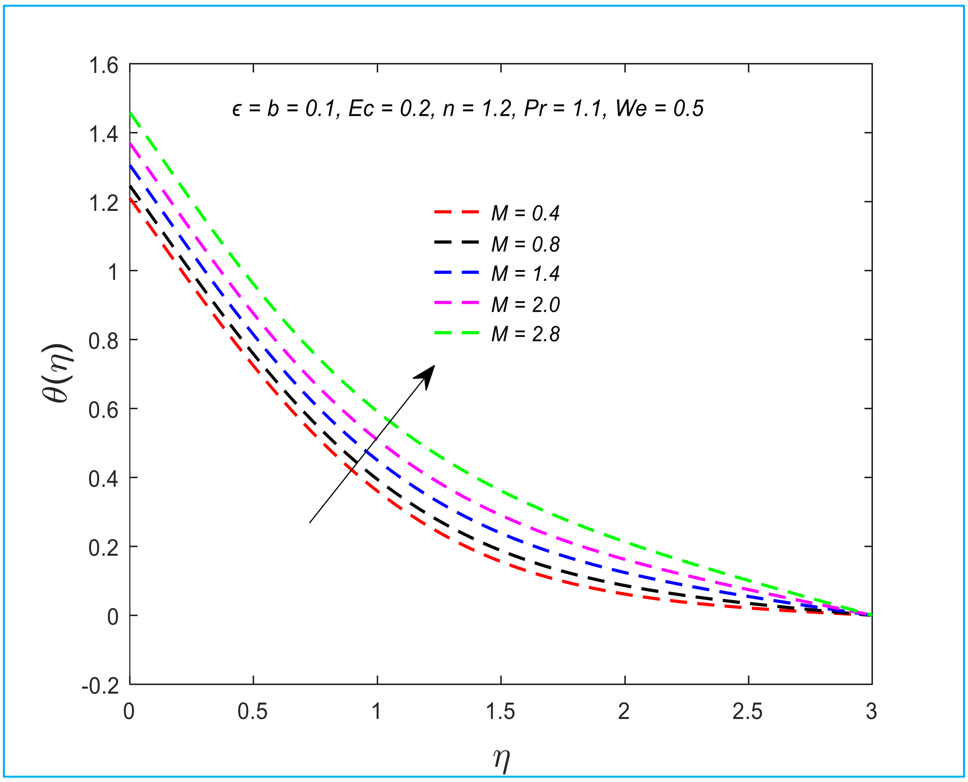

Fig. 11: Temperature distribution with magnetic body force number, M.

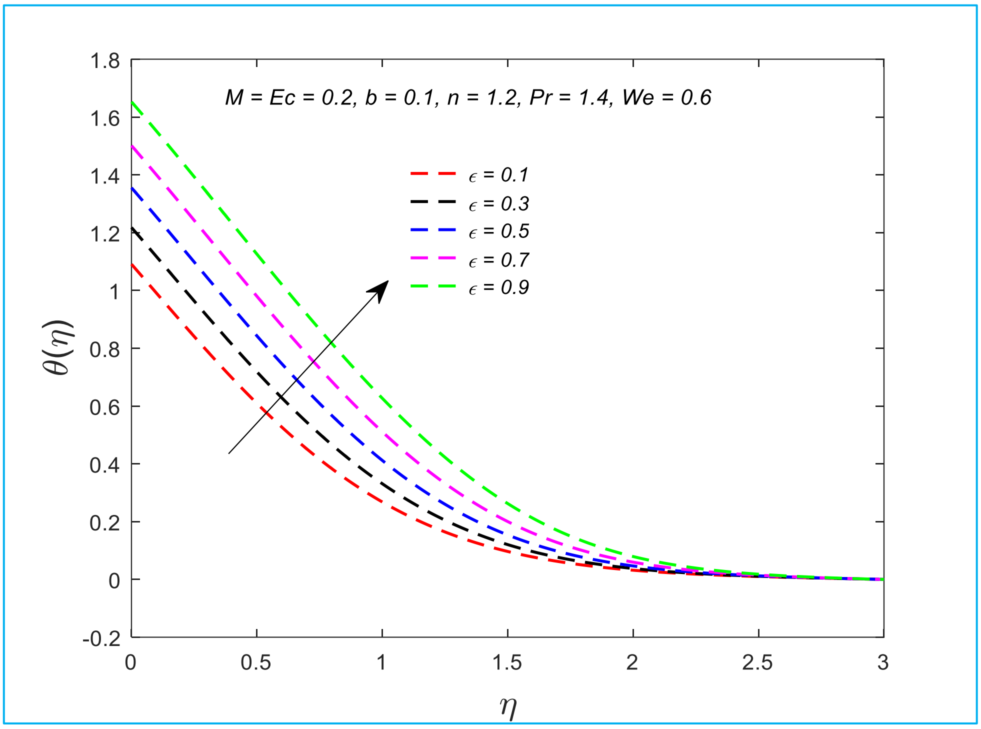

Fig. 12: Temperature distribution with thermal conductivity parameter, ε.

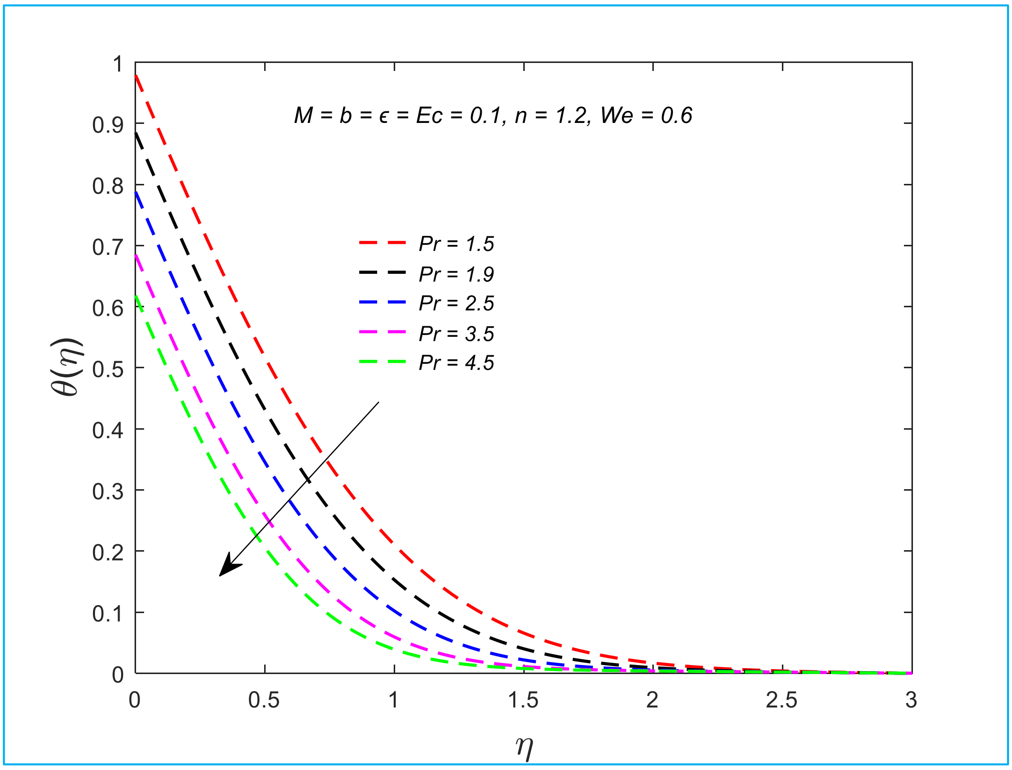

Fig. 13: Temperature distribution with Prandtl number, Pr.

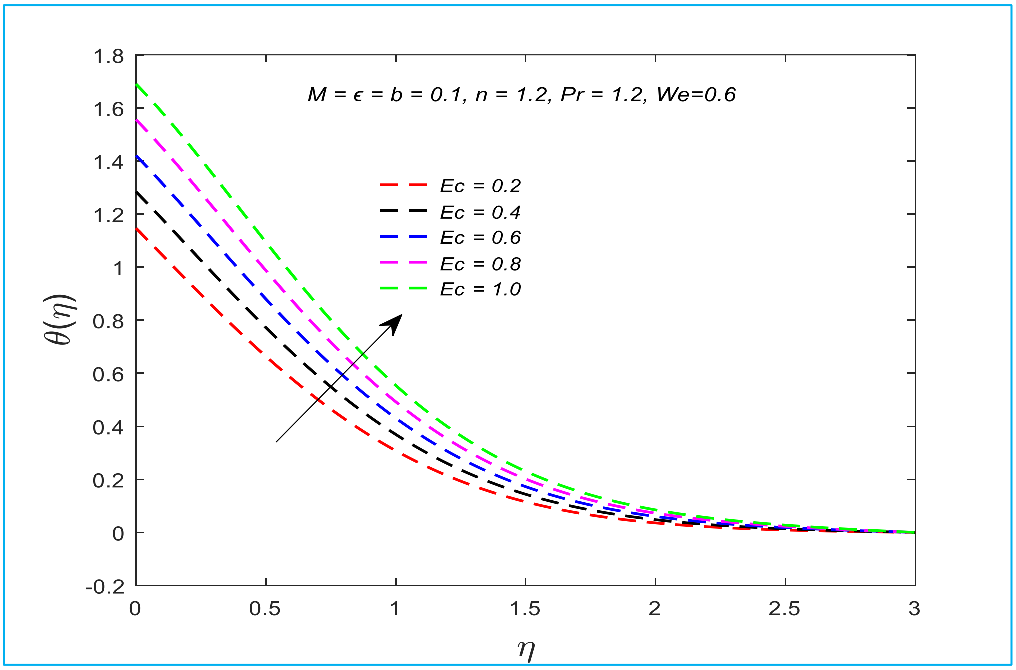

Fig. 14: Temperature distribution with Eckert number, Ec.

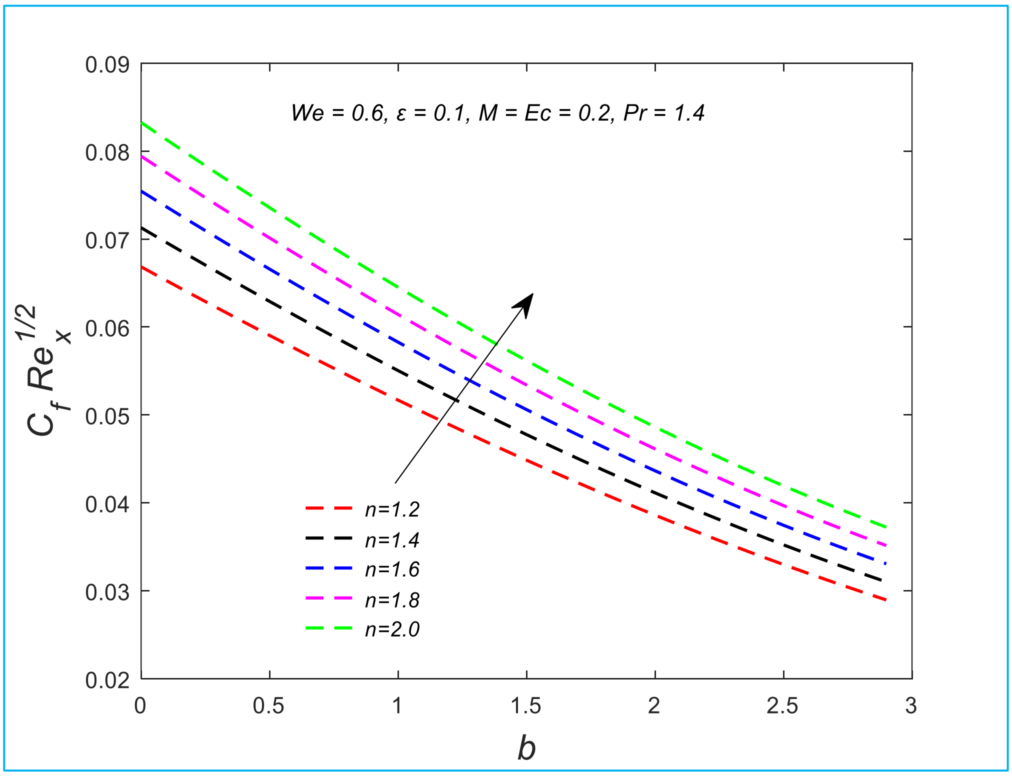

Fig. 15: Skin friction $C_f Re_x^{1/2}$distribution with with squeezing flow index, b and Carreau rheological power-law index, n.

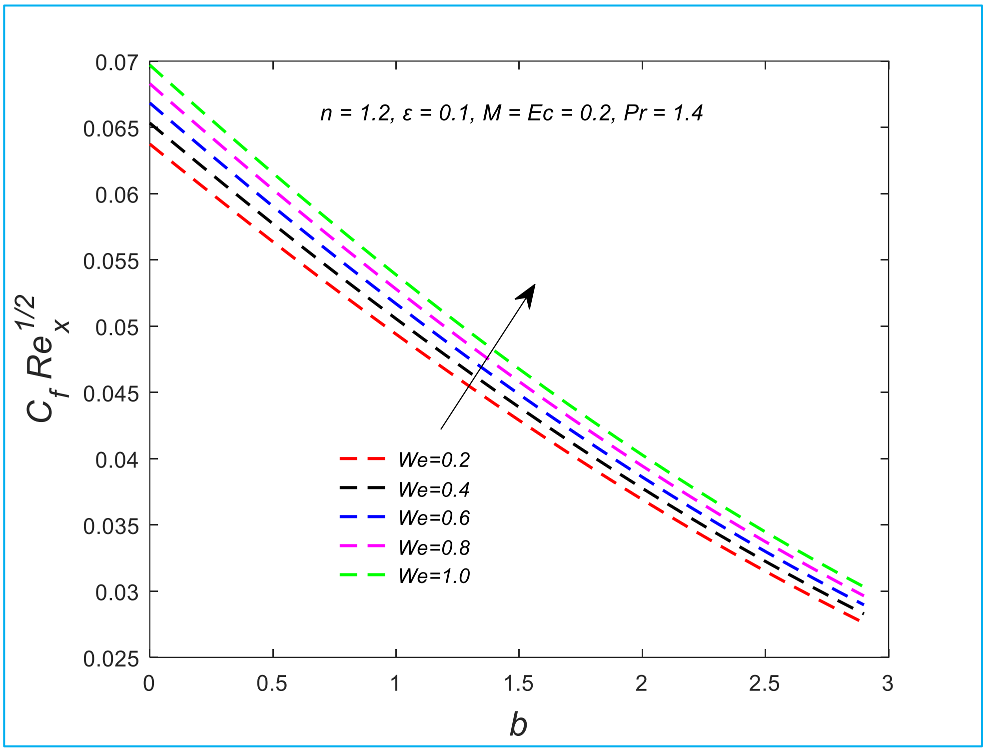

Fig. 16: Skin friction $C_f Re_x^{1/2}$distribution with with squeezing flow index, b and Weissenberg number, We.

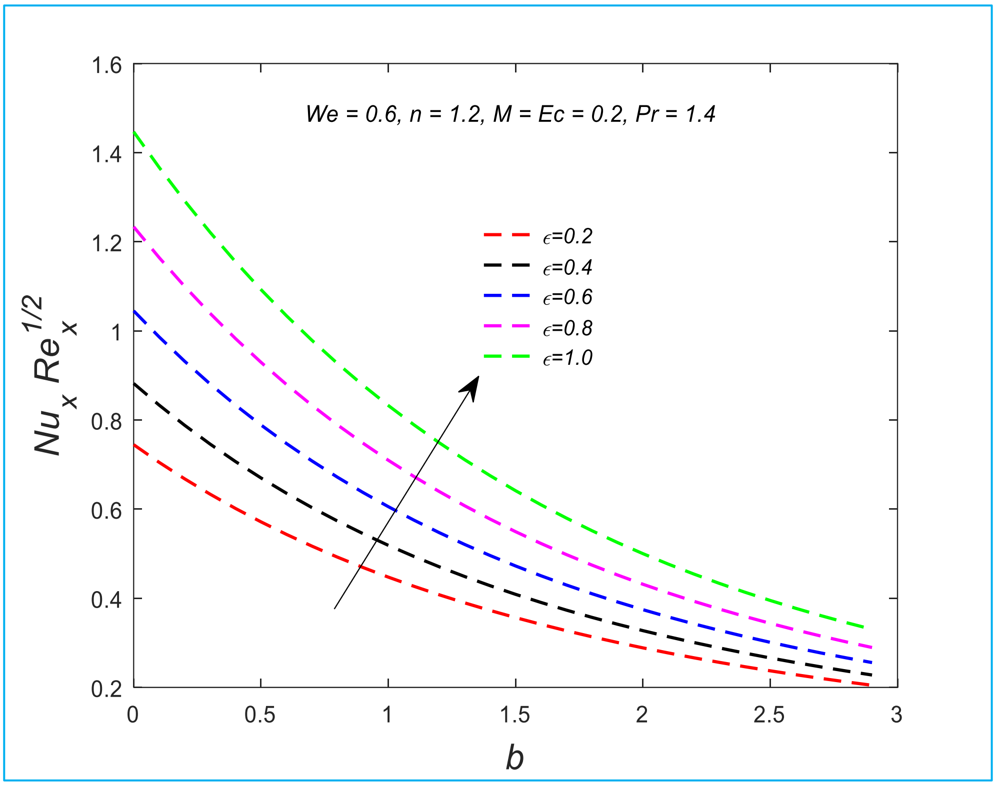

Fig. 17: Local Nusselt number $Nu_x Re_x^{1/2}$variation with squeezing flow index, b and thermal conductivity parameter, ε.

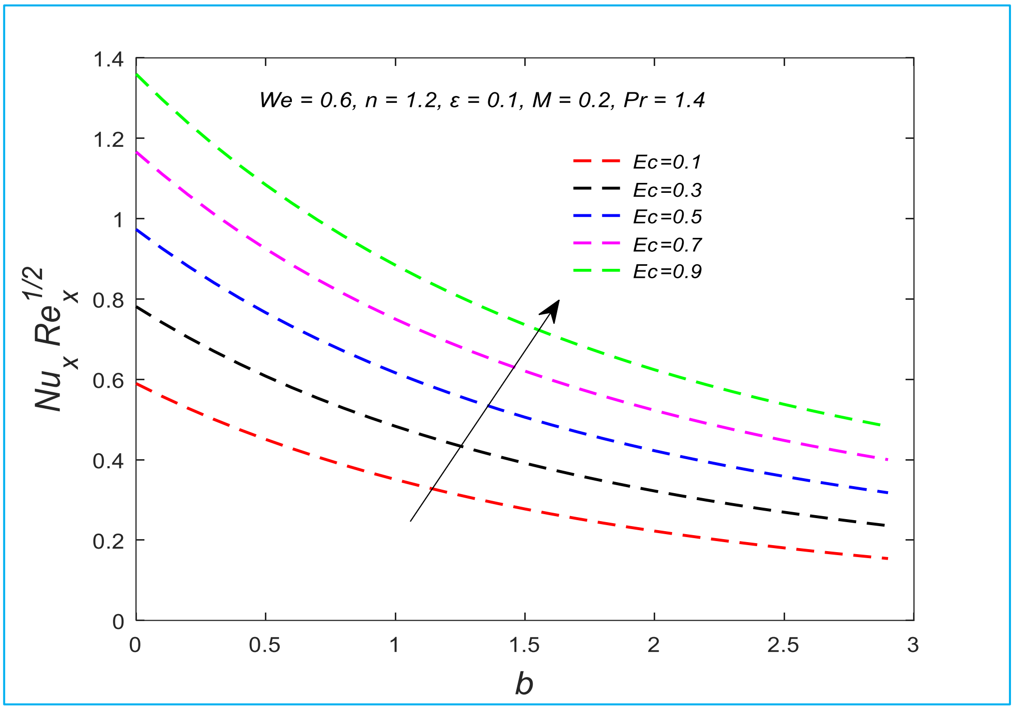

Fig. 18: Local Nusselt number $Nu_x Re_x^{1/2}$variation with with squeezing flow index, b and Eckert number, Ec.

Table 2. MATLAB RK4 computed skin-friction values.

n	b	We	f_o	M	ε	Ec	Pr	$C_f Re_x^{1/2}$
1.1	0.1	0.6	-0.2	0.1	0.1	0.1	1.2	1.243980
1.3								1.066636
1.5								0.934680
1.7								0.829049
1.2	0.0							1.163042
	0.2							1.131795
	0.4							1.098456
	0.6							1.062883
		0.1						1.320237
		0.3						1.243980
		0.5						1.177792
		0.7						1.119223
			-0.5					1.247156
			-0.3					1.181758
			-0.1					1.112850
			0.0					1.077446
			0.1					1.041621
			0.3					0.969384
			0.5					0.897502
				0.0				1.124270
				0.3				1.190630
				0.5				1.229108
				0.7				1.263736
					0.2			1.147672
					0.4			1.147672
					0.6			1.147672
					0.8			1.147672
						0.3		1.147672
						0.5		1.147672
						0.7		1.147672
						0.9		1.147672
							0.7	1.147672
							1.0	1.147672
							1.5	1.147672
							2.0	1.147672

Figures 2 and 3 illustrate the influence of Weissenberg parameter (We) on velocity and temperature distributions, respectively in the boundary layer regime. There is a strong decrement in velocity with increasing We. A monotonic growth is witnessed in all profiles from the wall to the freestream. We describes the relation of viscoelastic relaxation time to a specific time under which the fluid experiences shearing. It arises in the modified shear terms in the momentum boundary layer Eqn. (18) i.e. $\frac{3}{2}(n-1)We^2\left(f''(\eta)\right)^2 f'''(\eta)$. Greater values of We amplify the relaxation time of Carreau liquid i. e. a greater time is required for the fluid to relax when stress is removed. This delays the momentum diffusion in the regime and offers more opposition to the liquid motion over sensor sheet, resulting in deceleration in the flow. $We = ax\Omega\sqrt{\frac{a}{\nu}}$ and is clearly inversely proportional to the kinetic viscosity of the Carreau fluid. Higher values of *We* will also modify the viscosity, and this will also contribute to the modification in velocity evolution with transverse coordinate. Higher We will correspond to cases where the time scale of a flow is significantly smaller than the relaxation time of the elastico-viscous Carreau liquid, so that *elastic effects* dominate over viscous effects. However, for the opposite scenario, when relaxation time is much smaller than the time scale of the fluid, there is a depletion in elastic effects and the viscous effect becomes dominant. The range of values studied here is reflective of practical fluids deployed in micro-cantilever squeezing sensor designs which may span low values from *We* = 0.1 up to very high values approaching 10 [52]. The momentum boundary layer thickness is strongly increased with greater We and again this is directly associated with momentum diffusion inhibition in the regime. Conversely there is a distinct boost in temperatures induced with greater Weissenberg number, as observed in Fig. 3. The deceleration in the flow enables faster thermal diffusion in the fluid. The Prandtl number is designated as 1.2 for aqueous Carreau magnetic liquids in the simulation. Significant heating is therefore induced in the boundary layer and the thermal boundary layer thickness is increased. Although We does not arise explicitly in the energy Eqn. (19), via multiple nonlinear terms e. g. $Pr\left(f(\eta) + \frac{b\eta}{2}\right)\theta'(\eta)$, $-Pr\left(f'(\eta) + \frac{b}{2}\right)\theta(\eta)$, there is a marked indirect influence on the temperature field via coupling with the momentum field. A monotonic decay is computed in all profiles from the wall (where temperature is maximum) to the free stream (where it is a minimum). Asymptotically smooth profiles are achieved in both plots in the free stream confirming that a sufficiently large infinity boundary condition has been prescribed in the MATLAB RK-4 code.

Squeezing flow index (gap parameter) effect on velocity and temperature distributions

The impact of squeezing flow index (b) on velocity and temperature profiles with transverse coordinate (η) is depicted in **Figs. 4 and 5**, respectively. A substantial reduction in velocity is induced with amplifying values of b i. e. the flow is retarded, and momentum boundary layer thickness is enhanced. This is for initial values of η*; however, after a critical distance the reverse effect is observed with a slight acceleration which is sustained into the free stream.* There is an inverse relationship between the value of *b* and the proximity of the plates engulfing the micro-cantilever surface with squeezing flow. This is visible in the definition of the plates gap i. e. $h(t) = \frac{1}{(s+bt)^{1/b}}$. As noted earlier when b = 0 the plates are constrained at a fixed distance apart, h_o. As *b* increases, the plate gap is diminished. This induces a strong suppression in momentum development and decreases velocity magnitudes, as observed in Fig. 4. The parameter b features in the momentum Eqn. (18) in the terms, $+b(f'(\eta) - 1)$ and $\left(f(\eta) + \frac{b\eta}{2}\right)f''(\eta)$. Velocity evolution is therefore intimately affected by a change in *b*. Molecules of fluid are inhibited with strong squeezing (i. e. high *b* values). However due to momentum re-distribution, as the free stream is approached, acceleration is produced. Significant control of the boundary layer characteristics is therefore achieved by modification in the squeezing flow index, *b* which permits greater sensitivity to be achieved in micro-cantilever designs for biomedical devices. At maximum *b* value (= 4.6) the topology of the velocity profile is also altered significantly, in particular at low values of the transverse coordinate. A consistent decay in temperatures from the wall is computed in **Fig. 5**. Increasing values of squeezing flow index, *b* also produces a strong decrement in temperature magnitudes. However, this trend is sustained at all values of the transverse coordinate (η). The parameter *b* also arises in the energy Eqn. (19) in the terms, $+Pr\left(f(\eta)+\frac{b\eta}{2}\right)\theta'(\eta)$ and $-Pr\left(f'(\eta)+\frac{b}{2}\right)\theta(\eta)$, showing that temperature is *directly affected* also by change squeezing flow index, *b*. Thermal boundary layer thickness is therefore depleted consistently with stronger squeezing effect. The closer proximity of the plates and associated lower plate gap with greater squeezing flow index, *b*, will therefore cool the regime and suppress molecular conduction heat transfer effects. Again, it is noteworthy therefore that enhanced squeezing enables effective thermal management of the micro-cantilever sensor and strategic design of the gap distance can be exploited in producing more accurate calibrations in clinical applications [4].

Carreau rheological power-law index effect on velocity and temperature distributions

The influence of the Carreau rheological power-law index (n) on velocity and temperature evolution is visualized in **Figs. 6 and 7**. Only the dilatant i. e. shear-thickening case is considered for which *n* >1. Pseudoplastic behaviour (*n* <1) is not analysed. The shear terms in the momentum Eqn. (18) are significantly modified with dilatant behaviour, as observed in the high order hydrodynamic term, $\frac{3}{2}(n-1)We^2\big(f''(\eta)\big)^2 f'''(\eta)$. Momentum diffusion is stifled with greater shear-thickening effect and the boundary layer flow is retarded. This mechanism therefore also offers an excellent control mechanism for regulating the micro-cantilever sensor regime, without inducing flow reversal (back flow), since positive velocity values are sustained at all values of transverse coordinate over the full range of dilatant cases considered (*n* is varied from 1.2 to 4.8). Plug flow which arises in yield stress fluids however is not observed since the Carreau fluid is *viscoelastic* in nature, not *viscoplastic*. The suppression in momentum diffusion with increasing values of Carreau rheological power-law index (n), produces a simultaneous boost in thermal diffusion in the boundary layer. Heat moves more effectively in the strongly dilatant case (*n* = 4.8) than in the weakly dilatant case (*n* = 1.2), illustrating that excellent thermal control is attainable with judicious selection of strongly shear-thickening fluids. Thermal boundary layer growth and thickness are enhanced overall with increment in *n* values. Both graphs also confirm that smooth convergence of the solutions is achieved in the free stream and this further verifies the prescription of a sufficiently large infinity boundary condition in the MATLAB RK4 computations.

Permeable wall velocity effect on velocity and temperature distributions

Figs. 8 and 9 depict the response in velocity $f'(\eta)$ and temperature $\theta(\eta)$ with variation in the permeable wall velocity (f_o). This parameter is invoked via the sensor (micro-cantilever) surface boundary condition in Eqn. (20), viz $f(0)=-f_o$. For (f_o) > 0 as considered in these plots, suction i. e. removal of Carreau fluid through the sensor wall is considered. This inhibits lateral mass flux into the boundary layer domain and decelerates the flow, as observed in Fig. 8. Hydrodynamic (momentum) boundary layer thickness is therefore increased with larger values of f_o. Flow reversal is however not generated as positive values of velocity are sustained at all transverse coordinate values. Conversely, temperature is accentuated strongly with increment in f_o as displayed in Fig. 9. The adhesion of the boundary layer to the sensor surface restricts momentum diffusion. Thermal diffusion is therefore enhanced, and heat is transported more effectively through the regime. Thermal boundary layer thickness is therefore also increased. The imposition of larger permeable wall velocity (suction) has the opposite effect to greater squeezing flow index, *b*, which as noted earlier induces cooling in the domain. Again, it is evident that peak temperature is computed always at the sensor surface (wall) irrespective of the suction permeable velocity magnitude, although the most prominent elevation in temperature is observed at the wall with increment in permeable velocity value.

Magnetic body force parameter effect on velocity and temperature distributions

The influence of increment in magnetic number (M) on velocity and temperature is plotted in **Figs. 10 and 11**. The magnetic field influence is modified by the free stream effect and simulated via the modified linear Lorentz body force term, $M\left(1 - f'(\eta)\right)$ appearing in Eqn. (18). While conventionally transverse magnetic field enhancement induces deceleration in boundary layer flows, due to the free stream influence, the reverse effect is computed i. e. velocity is accentuated with increasing *M* values. Flow acceleration on the sensor surface is therefore generated with stronger magnetic field and flow retardation with weaker magnetic field. The magnetic parameter, $M = \frac{\sigma B_o^2}{\rho a}$ signifies the relative contribution of Lorentz magnetic body force to the inertial force in the boundary layer flow. When $M = 1$ both these forces are balanced. For $M < 1$ the inertial force dominates (weak magnetic field case) and for $M > 1$ the Lorentz force dominates (strong magnetic field case). The momentum distribution is clearly very sensitive to transverse magnetic field and significant manipulation of the boundary layer growth on the sensor surface can be achieved via adjustment of the magnetic field intensity. The most prominent modification in velocity is observed at intermediate distances from the sensor surface (wall). Of course, the sensor experiences squeezing from the exterior dual plate system with b = 0.2. The overwhelming effect of magnetic field however supersedes the squeezing regime influence and leads to a strong acceleration in the flow. Fig 11 shows that temperature is also boosted with increment in magnetic field. The magnetic field has a direct effect on the temperature field via the Joule dissipation term, $+PrEcM\left(f'(\eta)\right)^2$, which features in the energy eqn. (19). The supplementary work expended in dragging the Carreau fluid against the action of the free stream modified magnetic body force is dissipated as thermal energy via Joule heating. This leads to an exacerbation in temperatures and a thicker thermal boundary layer is developed on the sensor surface. This effect has been noted in several other works including Cramer and Pai [19], Sastry *et al.* [38].

Thermal conductivity, Prandtl and Eckert number effects on temperature distributions

Figs. 12-14 visualize the influence of thermal conductivity parameter (ε), Prandtl parameter (Pr) and Eckert number (*Ec*) on temperature evolution, respectively. The parameter, ϵ appears in several terms in the energy Eqn. (19) viz $\left(1+\epsilon\theta(\eta)\right)\theta''(\eta)$ and $+\epsilon\left(\theta'(\eta)\right)^2$. It enhances the effective thermal conductivity of the magnetic Carreau sensor fluid which assist thermal diffusion via augmented molecular conduction effects. This boosts the temperature and increases thermal boundary layer thickness. Clearly heat distribution is amplified by modification in thermal conductivity (Fig. 13) which can be achieved via multiple methods including doping the Carreau fluid with metallic nanoparticles, micron sized particles etc. Thermal management is therefore achievable via this methodology and can be used in conjunction with the squeezing effect to produce desired temperature fluctuations in the system, which may be tuned for specific biomedical applications [4]. The effect of increasing Prandtl number (*Pr*) is, as anticipated, to significantly reduce temperature magnitudes (Fig. 13). Values of Prandtl number studies here range from 1.5 to 4.5 [52]. Physically these correspond to aqueous-based polymeric Carreau liquids which have a greater momentum diffusivity relative to thermal diffusivity and work well as insulators rather than conductors. Prandtl number is also inversely proportional to thermal conductivity, for fixed values of viscosity and specific heat capacity. Higher Prandtl number liquids will therefore conduct heat much less effectively than lower Prandtl number fluids, although *Pr* will generally always be in excess of unity for viscoelastic aqueous polymers [52]. Substantial cooling of the sensor surface can be attained therefore via deployment of higher Prandtl number Carreau liquids. Fig. 14 shows that elevation in Eckert number significantly enhances temperatures throughout the boundary layer domain. The Eckert number features in both the viscous heating term, $PrEc\left(f''(\eta)\right)^2$ and in the Ohmic heating (Joule magnetic dissipation) term, $+PrEcM\left(f'(\eta)\right)^2$ discussed earlier. $Ec=\frac{U^2}{C_p\left(\frac{q_o x}{k}\right)\sqrt{\frac{\nu}{a}}}$ and signifies the relative contribution of kinetic energy dissipated in the flow to the boundary layer enthalpy difference. Even in incompressible non-Newtonian flows, dissipation is significant owing to the high viscosity of dilatant liquids (n = 1.2 in the computations). This produces a strong conversion of mechanical energy to heat and results in a marked enhancement in temperatures and much greater thermal boundary layer thickness. In other models of sensor squeezing engulfed boundary layer flows, viscous heating has previously been neglected. The present analysis demonstrates that neglection of viscous heating (and also Joule heating) leads to erroneous values for temperature, since it under-predicts the heat transmission in real non-Newtonian liquids. Therefore, the inclusion of both viscous heating and Joule heating, which are real effects in magnetic rheological liquids, is strongly justified to achieve more physically viable predictions of the thermal field generated.

Squeezing index, Carreau rheological power-law index and Weissenberg number effect on skin friction

To provide an insight into wall characteristics on the sensor surface, **Figs. 15 and 16** display the skin friction i.e. dimensionless shear stress profiles, $C_f Re_x^{1/2}$ with selected non-Newtonian and squeezing parameters. A linear decay is observed in Fig. 15, with increment in squeezing flow index (b). However a strong enhancment in skin friction accompanies an increment in Carreau rheological power-index, *n*. Highly dilatant liquids therefore achieve greater flow acceleration at the sensor surface. Larger b values correspond to stronger squeezing which contrains the regime around the micro-cantiliver and suppresses boundary layer development leading to flow deceleration. This reduces the rate at which the Carreau liquids shears along the sensor surface and produces a plummet in skin friction. The maximum skin friction is achieved for b = 0 (constant plate gap distance). Similarly in Fig. 16 the skin friction is found to decay strongly and again in a linear fashion with squeezing flow index (b), although magnitudes are somewhat lower for the corresponding b values in Fig. 15. Increasing Weissenberg number induces a strong acceleration in the flow i.e. increases velocity values. High Weissenberg number relates to a dominance of elastic tensile stresses in the lqiuid and a reduction of viscous force, leading to a significant acceleration and greater skin friction values. The viscoelasticity of the Carreau liquid and the interplay between elastic and viscous forces therefore contributes greatly to behaviour computed at the sensor surface.

Squeezing flow index, thermal conductivity parameter and Eckert number influence on local Nusselt number

Figs. 17 and 18 depict the evolution in local Nusselt number i.e. $Nu_x Re_x^{1/2}$ with several selected parameters. In Fig. 17 a, a substantial decay in local Nusselt number is generated with increment in the squeezing flow index (b). However with elevation in thermal conductivity parameter (ε) there is a noticeable boost in $Nu_x Re_x^{1/2}$. The temperature elevation produced with greater squeezing effect manifests in a supression in heat transferred to the sensor surface i.e. greater heat is transferred into the Carreau non-Newtonian boundary layer regime. Similary there is an elevation in heat transfer rate to the sensor surface (wall) as thermal conductivity is augmented via the relation, for temperature-dependent thermal conducvity i.e. $\alpha(T) = \alpha_\infty(1+\epsilon\theta)$. Local Nusselt number is therefore accentuated. The sensor surface (wall) is therefore heated with stronger squeezing effect and greater thermal conductivity of the Carreau fluid. Fig. 18 shows that increment in Eckert (dissipation) number also produces an upsurge in local Nusselt number, $Nu_x Re_x^{1/2}$ which is sustained at all values of the squeezing flow index (b), although slightly lower magnitudes are computed relative to Fig. 17.

Table 2 shows that with greater rheological power-law index, n, squeezing flow index, b, Weissenberg number, We and permeable flow (suction) velocity, f_o, skin friction coefficient$C_f Re_x^{1/2}$ is consistently diminished whereas it is amplified with greater values of magnetic body force number, M. The impact of thermal conductivity parameter (ε), Eckert number (Ec) and Prandtl number (Pr) is insignificant on skin friction coefficient and therefore these plots were omitted in the graphs also.

7. CONCLUSIONS

Numerical solutions have been presented using MATLAB Runge-Kutta quadrature (RK-4) to compute the thermo-fluid characteristics in unsteady two-dimensional incompressible, laminar boundary layer flow of a magnetic Carreau liquid on a micro-cantilever sensing surface engulfed in a squeezing regime between parallel plates. The study has been motivated by characterizing more accurately the effects of viscous and Joule heating and also wall suction (a permeable sensor surface) and variable thermal conductivity on transport phenomena in biological MHD sensor systems. The principal findings of the current study may be summarized as follows:

- The flow velocity is shown to be strongly reduced and the momentum (hydrodynamic) boundary layer thickness significantly enhanced with greater values of Weissenberg viscoelastic number (ratio of stress relaxation time to process time).
- Temperature and thermal boundary layer thickness are boosted with increasing Weissenberg parameter.
- A strong deceleration in the boundary layer flow is induced with greater squeezing effect and temperature is also suppressed.
- Increasing magnetic interaction number accelerates the flow due to the free stream effect and also enhances temperatures and produces a thicker thermal boundary layer.
- Temperature is significantly elevated with increment in Eckert number via the viscous dissipation and Joule heating contributions.
- Flow retardation is induced with stronger suction at the sensor surface (wall) whereas temperatures are elevated.
- Skin friction coefficient is boosted with greater Carreau power-law rheological index (dilatant shear thickening behaviour) but suppressed with stronger squeezing effect.
- Nusselt number is magnified with greater thermal conductivity parameter and Eckert number but decays with greater squeezing effect.

The current study has also demonstrated that the Matlab-based RK-4 numerical approach is a very efficient procedure for simulating nonlinear magnetohydrodynamic non-Newtonian flows in sensor devices. However, attention has been confined to the Carreau model. Furthermore, electrical field effects have been ignored as have magnetic induction effects. Future studies may consider the combined electro-magnetic control mechanism for biomedical micro-cantilever flows and consider alternative rheological models such as the Stokes' couple stress (polar) model and the Walters-B short memory model which are also appropriate for electroconductive polymers deployed in modern biomedical sensors. Efforts in this direction and are currently underway and will be reported imminently.

Acknowledgements:

The first author wishes to express his gratitude to the Department of Science and Technology, Government of India for the granting of DST-Inspire Fellowship (IF190169) (Grant no. C/4084/IFD/2020-21) and to the Central University of Karnataka for providing the research facilities. The authors wish to express their gratitude to the reviewers who highlighted important areas for improvement in the earlier draft of this article. Their suggestions have served specifically to enhance the clarity and depth of the interpretation of results in the revised manuscript.

Data Availability Statement: Not Applicable (N/A). This manuscript has No Associated Data.

REFERENCES

[1] Lawal, A., and Kalyon, D. M., Squeezing flow of viscoplastic fluids subject to wall slip, *Polymer Engineering & Science*, 38(11) (1988) 1793-1804.

[2] Xu, C., Yuan, L., Xu, Y., and Hang, W., Squeeze flow of interstitial Herschel-Bulkley fluid between two rigid spheres, Particuology, 8 (2010) 360-364.

[3] Engmann, J., Servais C., and Burbidge, A. S., Squeeze flow theory and applications to rheometry: A review, *Journal of Non-Newtonian Fluid Mechanics*, 132(2005) 1-27.

[4] Zhang, X., Ju, H., and Wang, J., *Electrochemical Sensors, Biosensors and their Biomedical Applications*, Academic Press, USA (2008).

[5] Gupta, P. S., and Gupta, A. S., Squeezing flow between parallel plates. *Wear,* 45, 177–185, 1977.

[6] Kuzma, D. C., Fluid inertia effects in squeeze films, *Applied Science Research*, 18 (1967) 15-20.

[7] Wang, C. Y., and Watson, L. T., Squeezing of a viscous fluid between elliptic plates, *Applied Science Research*, 35 (1979) 195-207.

[8] Usha, R., and Sridharan, R., Arbitrary squeezing of a viscous fluid between elliptic plates, *Fluid Dynamics Research*, 18 (1996) 35-51.

[9] A. G. Petrov and I. S. Kharlamova, The solutions of Navier–Stokes equations in squeezing flow between parallel plates, *European Journal of Mechanics - B/Fluids*, 48, 40-48 (2014).

[10] Mustafa, M., Hayat, T., and Obaidat, S., On heat and mass transfer in the unsteady squeezing flow between parallel plates, *Meccanica*, 47 (2012) 1581-1589.

[11] Hayat, T., Sajjad, R., Alsaedi, A., Muhammad, T., and Ellahi, R., On squeezed flow of couple stress nanofluid between two parallel plates, *Results in Physics*, 7 (2017) 553-561.

[12] T. Hayat, M. Hussain, S. Nadeem, S. Obaidat, Squeezed flow and heat transfer in a second-grade fluid over a sensor surface, *Therm. Sci.*, 18 (2014), pp. 357-364.

[13] O. Anwar Bég, Walid S. Jouri, Tasveer A. Bég, Ali Kadir, Henry J. Leonard, M.D. Shamshuddin and T.K. Hung, Computation of asymmetric micropolar squeezing flow in a bionic prosthetic dual disk system with blowing (injection) and Reynolds number effects, *Int. Conf. Advances in Mathematics, Physics & Applied Science (ICAMPA), New Delhi, India, March 1st* (2020).

[14] L. Fusi *et al.*, Planar squeeze flow of a Bingham fluid, *Journal of Non-Newtonian Fluid Mechanics*, 225, 1-9 (2015).

[15] M. B. Arain, M. M. Bhatti, A. Zeeshan, F. Alzahrani and O. Anwar Bég, Radiative bioconvection nanofluid squeezing flow between rotating circular plates: semi-numerical study with the DTM-Padé approach, *Modern Physics Letters B.* (2021). (2021). 2150552 (22 pages) DOI: 10.1142/S0217984921505527

[16] Uddin, J., Marston, J. O., and Thoroddsen, S. T., Squeeze flow of a Carreau fluid during sphere impact, *AIP Physics of Fluids*, 24, 073104, 2012.

[17] L. Panina and K. Mohri, Magneto-impedance in multilayer films, *Sensors Actuators A*, vol. 81, pp. 71-77 (2000).

[18] A. Alfadhel, B. Li, A. Zaher, O. Yassine and J. Kosel, Magnetic nanocomposite for biomimetic flow sensing, *Lab Chip, The Royal Society of Chemistry (RSC)*, 14, 4362-4369 (2014).

[19] K.C. Cramer and S.I. Pai, *Magnetofluid Dynamics for Engineers and Applied Physicists*, MacGraw-Hill, New York, USA (1973).

[20] D.C. Kuzma, Magnetohydrodynamic squeeze films, ASME *J. Basic Eng*. 86(3): 441-444 (1964).

[21] Bhattacharyya, S., and Pal, A., Unsteady MHD squeezing flow between two parallel rotating discs, *Mechanics Research Communications*, 24(6) (1997) 615-623.

[22] J.C. Umavathi, S.L. Patil, B. Mahanthesh and O. Anwar Bég, Unsteady squeezing flow of magnetized nano-lubricant between parallel disks with Robin boundary condition, *Proc. IMechE J. Nanomaterials, Nanoengineering and Nanosystems* (2020). DOI: 10.1177/239779 14211036562 (15 pages)

[23] O. Anwar Bég, M.M. Rashidi, T. A. Bég and M. Asadi, Homotopy analysis of transient magneto-bio-fluid dynamics of micropolar squeeze film: *a model for magneto-bio-rheological lubrication, J. Mechanics In Medicine and Biology,* 12 (3) 1250051-1 to 1250051-21, (2012).

[24] O. Anwar Bég, D. Tripathi, T. Sochi and PK Gupta, Adomian decomposition method (ADM) simulation of magneto-biotribological squeeze film with magnetic induction effects, *J. Mechanics Medicine Biology,* 15, 1550072.1-1550072.23 (2015).

[25] M. Shamshuddin, S.R. Mishra, Ali Kadir and O. Anwar Bég, Unsteady chemo-tribological squeezing flow of magnetized bioconvection lubricants: *numerical study, J. Nanofluids*, 8 (2) 407-419 (2019).

[26] Khan, M., Qayyum, M., Khan, O., and Ali, M., Unsteady squeezing flow of Casson fluid with magneto-hydrodynamic effect and passing through porous medium, *Mathematical Problems in Engineering*, 2016, 1-14 (2016).

[27] Salahuddin, T., Malik, M. Y., Hussain, A., Bilal, S., Awais, M., and Khan, I., MHD squeezed flow of Carreau-Yasuda fluid over a sensor surface, *Alexandria Engineering Journal*, 56, 27-34 (2017).

[28] P. G. Datskos *et al.*, Detection of 2-mercaptoethanol using gold-coated micromachined cantilevers, *Sensors and Actuators B: Chemical*, 61, 75-82 (1999).

[29] N.V. Lavrik, C.A. Tipple, M.J. Sepaniak, D. Datskos, Gold nanostructures for transduction of biomolecular interactions into micrometer scale movements, *Biomed. Microdev.* 3 (1) 35–44 (2001).

[30] A.-R.A. Khaled and K. Vafai, Hydromagnetic squeezed flow and heat transfer over a sensor surface, *International Journal of Engineering Science*, 42, 509–519 (2004).

[31] Usha S., and Naduvinamani, N. B., Magnetized squeezed flow of time-dependent Prandtl-Eyring fluid past a sensor surface, *Heat Transfer-Asian Research*, 48, 2237-226 (2019).

[32] C. Kolitawong *et al.*, Viscous dissipation of a power law fluid in axial flow between isothermal eccentric cylinders, *Journal of Non-Newtonian Fluid Mechanics*, 166, 133-144 (2011).

[33] K. M. Awati *et al.*, Wall slip and shear stresses of polymer melts at high shear rates without pressure and viscous heating effects, *Journal of Non-Newtonian Fluid Mechanics*, 89, 117-131 (2000).

[34] J. Sheela-Francisca *et al.*, Heat transfer on asymmetric thermal viscous dissipative Couette–Poiseuille flow of pseudo-plastic fluids, *Journal of Non-Newtonian Fluid Mechanics*, 169/170, 42-53 (2012).

[35] S. S. Ghadikolaei et al., Analysis of unsteady MHD Eyring-Powell squeezing flow in stretching channel with considering thermal radiation and Joule heating effect using AGM, *Case Studies in Thermal Engineering*, 10, 579-594 (2017).

[36] U. Khan *et al*., Effects of viscous dissipation and slip velocity on two-dimensional and axisymmetric squeezing flow of Cu-water and Cu-kerosene nanofluids, *Propulsion and Power Research*, 4, 40-49 (2015).

[37] H.M. Duwairi *et al.*, On heat transfer effects of a viscous fluid squeezed and extruded between two parallel plates, *Heat and Mass Transfer*, 41, 112–117 (2004).

[38] R. V. S. R. K. Sastry D, Naresh Kumar N, Sivaraj R, *et al.* Unsteady MHD flow of a micropolar nanofluid through a dilating channel in the presence of ohmic heating. *Authorea.* (2020). DOI: 10.22541/au.159144666.60068871

[39] S.R. Mishra, MD. Shamshuddin, O. Anwar Bég and A. Kadir, Viscous dissipation and Joule heating effects in non-Fourier MHD squeezing flow, heat and mass transfer between Riga plates with thermal radiation: *variational parameter method solutions, Arabian J. Science Engineering*, 44, 8053–8066 (2019).

[40] M. Zubair *et al.*, Entropy Generation optimization in squeezing magnetohydrodynamics flow of Casson nanofluid with viscous dissipation and Joule heating effect, *Entropy*, *21*(8), 747-756 (2019). https://doi.org/10.3390/e21080747.

[41] Magodora, M., Mondal, H., Motsa, S., and Sibanda, P., Numerical studies on gold water nanofluid flow with activation energy past a rotating disk, *International Journal of Applied and Computational Mathematics*, 8, 41 (2022) (DOI: 10.1007/s40819-022-01241-4).

[42] Almakki, M., Mondal, H., Mburu, Z., and Sibanda, P., Entropy generation in double diffusive convective magnetic nanofluid flow in rotating sphere with viscous dissipation, *Journal of Nanofluids*, 11, 360-372 (2022).

[43] Almakki, M., Mondal, H., and Sibanda, P., Onset of unsteady MHD micropolar nanofluid flow with entropy generation, *International Journal of Ambient Energy*, 2022, (DOI: 10.1080/01430750.2021.1890213) (Ahead of print).

[44] Dhlamini, M., Mondal, H., Sibanda, P., and Motsa, S., Activation energy and entropy generation in viscous nanofluid with higher order chemically reacting species, *International Journal of Ambient Energy*, 43(1), 1495-1507 (2022).

[45] Sithole, H., Mondal, H., Magagula, V. M., Sibanda, P., and Motsa, S., Bivariate Spectral Local Linearization Method (BSLLM) for unsteady MHD micropolar-nanofluids with

homogeneous–heterogeneous chemical reactions over a stretching surface, *International Journal of Computational Mathematics*, 5(12), 1-14 (2019).

[46] Khan, M., Malik, M. Y., Salahuddin, T., and Khan, I., Heat transfer squeezed flow of Carreau fluid over a sensor surface with variable thermal conductivity: A numerical study, *Results in Physics*, 6, 940-945 (2016).

[47] Kumar, K. G., Gireesha, B. J., Krishanamurthy, M. R., and Rudraswamy, N. G., An unsteady squeezed flow of a tangent hyperbolic fluid over a sensor surface in the presence of variable thermal conductivity, *Results in Physics*, 7, 3031-3036 (2017).

[48] Usha S., Naduvinamani, N. B., and Basha, H., Effect of magnetized variable thermal conductivity on flow and heat transfer characteristics of unsteady Williamson fluid, *Nonlinear Engineering*, 9, 338–351 (2020).

[49] Basha, H., A generalized perspective of magnetized radiative squeezed flow of viscous fluid between two parallel disks with suction and blowing, *Heat Transfer-Asian Research*, 49, 2248-2281 (2020).

[50] O. Anwar Bég, Numerical methods for multi-physical magnetohydrodynamics, Chapter 1, pp. 1-112, *New Developments in Hydrodynamics Research, M. J. Ibragimov and M. A. Anisimov, Eds*., *Nova Science, New York, USA* (2012).

[51] Usha, S., Naduvinamani, N. B., and Basha, H., A generalized perspective of Fourier and Fick's laws: Magnetized effects of Cattaneo-Christov models on transient nanofluid flow between two parallel plates with Brownian motion and thermophoresis, *Nonlinear Engineering*, 9, 201-222 (2020).

[52] T. Mezger, *The Rheology Handbook*, Vincentz Network, Germany (2020).